Global Change Biology (2005) **11,** 335–355, doi: 10.1111/j.1365-2486.2005.00897.x

Estimating diurnal to annual ecosystem parameters by synthesis of a carbon flux model with eddy covariance net ecosystem exchange observations

BOBBY H. BRASWELL*, WILLIAM J. SACKS†, ERNST LINDER‡, and DAVID S. SCHIMEL§
Complex Systems Research Center, University of New Hampshire, Durham, NH 03824, USA, †Department of Environmental Studies, Williams College, P.O. Box 632, Williamstown, MA 01267, USA, ‡Department of Mathematics and Statistics, University of New Hampshire, Durham, NH 03824, USA, §Climate and Global Dynamics Division, National Center for Atmospheric Research, P.O. Box 3000, Boulder, CO 80305, USA

Abstract

We performed a synthetic analysis of Harvard Forest net ecosystem exchange of CO_2 (NEE) time series and a simple ecosystem carbon flux model, the simplified Photosynthesis and Evapo-Transpiration model (SIPNET). SIPNET runs at a half-daily time step, and has two vegetation carbon pools, a single aggregated soil carbon pool, and a simple soil moisture sub-model. We used a stochastic Bayesian parameter estimation technique that provided posterior distributions of the model parameters, conditioned on the observed fluxes and the model equations. In this analysis, we estimated the values of all quantities that govern model behavior, including both rate constants and initial conditions for carbon pools. The purpose of this analysis was not to calibrate the model to make predictions about future fluxes but rather to understand how much information about process controls can be derived directly from the NEE observations. A wavelet decomposition enabled us to assess model performance at multiple time scales from diurnal to decadal. The model parameters are most highly constrained by eddy flux data at daily to seasonal time scales, suggesting that this approach is not useful for calculating annual integrals. However, the ability of the model to fit both the diurnal and seasonal variability patterns in the data simultaneously, using the same parameter set, indicates the effectiveness of this parameter estimation method. Our results quantify the extent to which the eddy covariance data contain information about the ecosystem process parameters represented in the model, and suggest several next steps in model development and observations for improved synthesis of models with flux observations.

Keywords: Bayesian analysis, data assimilation, Markov Chain Monte Carlo (MCMC) methods, net ecosystem exchange (NEE), parameter estimation, terrestrial carbon cycle

Received 15 September 2003; revised version received 18 March 2004 and accepted 27 September 2004

Introduction

Direct measurements of net ecosystem exchange of CO_2 (NEE) using eddy covariance provide clear evidence that carbon fluxes are responsive to a range of environmental factors. NEE data document the sensitivity of fluxes to both site conditions and climatic variability (Goulden *et al.*, 1996; Law *et al.*, 2003). However, because NEE is the difference between photosynthesis and respiration, direct inference of process controls from flux data remains a technical challenge, dependent on the assumptions used to separate the net flux into its components. The goal of this paper is to use estimation procedures to determine how much information about state variables (such as leaf area), rate constants (such as temperature coefficients) and thresholds (such as critical temperatures for photosynthesis) can be obtained directly and simultaneously from the eddy covariance record.

We analyzed the decadal Harvard Forest record using a model-data synthesis or 'data assimilation' approach, combining observations with an ecosystem model. The model we used in this study is based on the

Correspondence: Bobby H. Braswell, tel. 603 862 2264, fax 603 862 0188, e-mail: rob.braswell@unh.edu

© 2005 Blackwell Publishing Ltd

Photosynthesis and Evapo-Transpiration (PnET) family of ecosystem models (Aber & Federer, 1992), which were designed to be compared with eddy flux data (Aber *et al*., 1996). In this analysis, we estimate both the optimal parameter values (rate constants and thresholds) and the initial conditions for the state variables by minimizing the deviation between observed and simulated fluxes. Initial conditions and simulation of state variables can have significant effects on models results, especially in biogeochemistry, where currently most attention is focused on rate constant estimation (e.g. Giardina & Ryan, 2000). Recognizing this, we placed as much emphasis on estimating the initial carbon pools as on estimating the other model parameters.

In performing the parameter estimation, we used a Bayesian approach. The cornerstone of Bayesian statistics is Bayes' theorem (Gelman *et al*., 1995), which provides a mechanism for obtaining posterior distributions of model parameters that combine information from the data (by defining likelihood in terms of model error) and from assumed prior parameter distributions. Recent advances, enabled by increasing computer power, such as the application of Markov Chain Monte Carlo (MCMC) methods, have provided a solution to the problem of searching high dimensional parameter spaces. In this approach, ecosystem model parameters and data uncertainty are all treated as probability distributions. Conclusions about the information content of the data and about model validity are made by inspection of the posterior distributions.

The relative importance of different ecosystem processes varies from diurnal to seasonal to interannual time scales, and the information content of the data may also vary across time scales. Terrestrial models have previously been combined with inference techniques to estimate the role of processes operating at multiple time scales through state and parameter estimation techniques (Luo *et al*., 2001; Vukicevic *et al*., 2001), and flux data are increasingly being used to make inferences about controls over processes on these multiple time scales (e.g. Baldocchi & Wilson, 2001). The Harvard Forest eddy covariance data record, the longest such record available, should contain information about controls over carbon fluxes on all these time scales. Inferences about controls on the diurnal time scale are relatively straightforward since they can draw on many observations. As the time scale lengthens towards seasonal and interannual scales, however, statements about process-level controls become more uncertain (Goulden *et al*., 1996), aggravated by the smaller number of 'replicate' seasonal and year-to-year patterns than daily cycles. As we obtain longer records of NEE from eddy covariance sites, this uncertainty will gradually diminish.

The impact of the data on parameters governing different time scales and the goodness of fit on different time scales can be analyzed after assimilation into a model. This type of analysis combines empirical analysis of the data with comparison of the data to theory, as embodied in the model structure. We present a systematic analysis of model performance on multiple time scales using wavelet decomposition.

Methods

In this section, we describe the processing of the eddy flux and meteorological data, the development of the ecosystem carbon flux model, and the parameter estimation scheme. Two overarching design constraints affected all aspects of the experiment. First, we chose to perform the analyses at a half-daily time step. Thus, the model and data were designed to consider each alternating daytime and nighttime interval as two discrete steps, with the length of each time step based on a calculation of sunrise and sunset times. This condition fixes the overall data volume, and to some extent the degree of process-level aggregation. However, the daytime and nighttime points were considered together, as a single data set, in the parameter estimation. Most similar ecosystem models are run using a time step of a day (e.g. Aber *et al*., 1996; Parton *et al*., 1998) or longer (e.g. Raich *et al*., 1991; Potter *et al*., 1993). Using a half-daily time step, however, gives time steps in which photosynthesis is not occurring, and thus the only carbon fluxes are from respiration. This facilitates the separation of respiration processes from photosynthesis in the data assimilation, since nighttime data provide leverage on only the respiration-related parameters. Second, we chose to begin with a model that represents relatively few processes, so that we could easily evaluate the degree to which the data provide leverage on the parameterization of each process.

Data overview and processing

Eddy flux estimates of net ecosystem exchange are based on the covariance of high frequency fluctuations in vertical wind velocity and CO_2 concentration (Baldocchi *et al*., 1988). Though there is now a global network of these tower-based monitoring sites, the longest record is available at the Harvard Forest Long-Term Ecological Research (LTER) site near Petersham, Massachusetts, USA (Wofsy *et al*., 1993; Goulden *et al*., 1996). Starting in late 1991, quality-controlled estimates of NEE have been available at hourly time intervals, along with a suite of other meteorological variables. In our analysis, we used the hourly observations of eddy

13652486, 2005, 2, Downloaded from https://onlinelibrary.wiley.com/doi/10.1111/j.1365-2486.2005.00897.x by University Of Arizona Library, Wiley Online Library on [24/07/2024]. See the Terms and Conditions (https://onlinelibrary.wiley.com/terms-and-conditions) on Wiley Online Library for rules of use; OA articles are governed by the applicable Creative Commons License

flux, canopy CO_2 storage, humidity, photosynthetically active radiation (PAR), air temperature, air pressure, soil temperature, and momentum flux, from 1992 to 2001. Since hourly precipitation data were not available, we used daily precipitation observations, which are a composite of representative data from area weather stations. All the hourly meteorological data were averaged within the daytime and nighttime intervals for each day. The daily precipitation data were subdivided into two equal intervals per day.

Net ecosystem exchange was calculated by addition of the eddy flux values with the mean storage changes observed at five vertical levels. We calculated the friction velocity (U^*) from the momentum flux, and vapor pressure deficit (VPD) from the relative humidity and air pressure. Gaps in the carbon exchange and meteorological data were filled using multivariate nonlinear regression (MacKay, 1992; Bishop, 1995) based on the available meteorological data, the day of year, and the time of day. Although gap-filled data are available at a daily time step (Falge *et al*., 2001), we needed hourly values in order to calculate daytime and nighttime sums. Because only 14% of the half-daily time steps contained no gap-filled data, it was necessary to include some gap-filled points in the optimization to obtain a sufficient quantity of data. Including all gap-filled points, however, would have given too much weight to the modeled data points, and too little weight to the measured data. As a compromise, we applied a filter to the data so that only the half-daily intervals with 50% or fewer missing values were included in the model-data comparison.

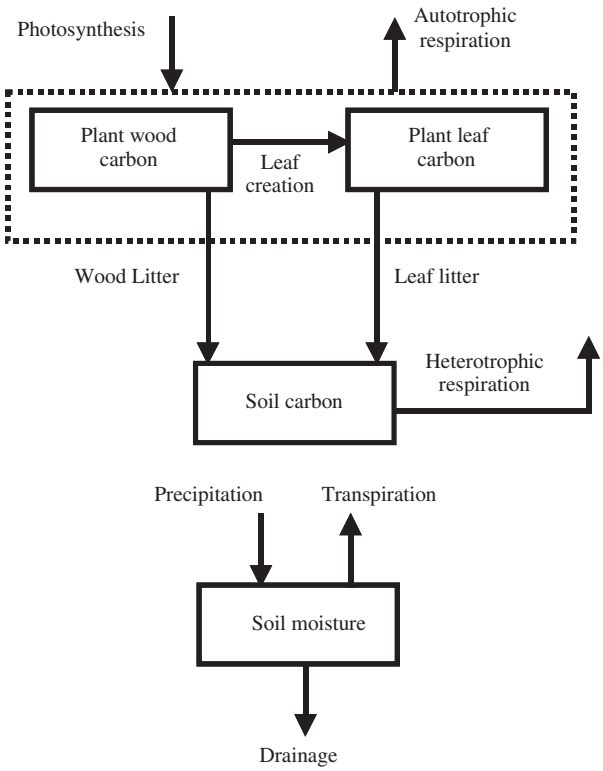

Fig. 1 Simplified PnET model pools and fluxes. The model has two vegetation carbon pools and one soil carbon pool. Photosynthesis and autotrophic respiration actually add to and subtract from the plant wood carbon pool, but can alternatively be thought of as modifying the plant leaf carbon pool, with balancing flows of carbon between the wood pool and the leaf pool to keep the leaf pool constant over the growing season. The soil moisture sub-model affects photosynthesis and soil respiration.

Ecosystem model and parameters

We used a simplified version of the PnET ecosystem model (Aber & Federer, 1992). A number of variants of this model are available, and we chose to start from a daily time-step version (PnET-Day), which has been compared extensively with Harvard Forest NEE data (Aber *et al*., 1996). We chose this model partly because of its history of use in northern temperate forest ecosystems and with eddy flux data, and partly because of its moderate level of complexity. We constructed the simplified PnET model (SIPNET) (Fig. 1) as a new model, rather than starting from existing code, for easier integration of the model equations with the other parts of the assimilation scheme. This approach allowed for easier incorporation of sub-components from other models. The model is formulated as a set of coupled ordinary differential equations, which were solved using Euler's method for computational efficiency.

There are four major differences between SIPNET and PnET-Day. First, we simulate processes twice per day. Second, we replaced the carbon-economic scheme of Aber *et al*. (1996) for determining canopy leaf area index (LAI) development with a simple parametric phenology that signals foliar production and senescence based on either the day of year (in most model runs), or on degree-day accumulation (in one case). Canopy foliar development and senescence each occur in a single time step. Third, as in TEM (Raich *et al*., 1991), we model wood maintenance respiration as a function of wood carbon content and temperature. Finally, as in PnET-CN (Aber *et al*., 1997), we model heterotrophic respiration as a function of soil carbon content, soil temperature and soil moisture.

At each time step, NEE is computed as:

$$\mathrm{NEE} = R_a + R_h - \mathrm{GPP}, \quad (1)$$

where R_a is the autotrophic respiration, R_h is heterotrophic respiration, GPP is gross photosynthesis, and

13652486, 2005, 2, Downloaded from https://onlinelibrary.wiley.com/doi/10.1111/j.1365-2486.2005.00897.x by University Of Arizona Library, Wiley Online Library on [24/07/2024]. See the Terms and Conditions (https://onlinelibrary.wiley.com/terms-and-conditions) on Wiley Online Library for rules of use; OA articles are governed by the applicable Creative Commons License

Table 1 SIPNET parameters and initial conditions

Symbol	Definition	Units
Initial pool values		
$C_{W,0}$	Initial plant wood C content	$g\,C\,m^{-2}$
$C_{L,0}$	Initial plant leaf C content	$g\,C\,m^{-2}$
$C_{S,0}$	Initial soil C content	$g\,C\,m^{-2}$
W_0	Initial soil moisture content	cm (precipitation equivalent)
Photosynthesis parameters		
A_{max}	Maximum net CO_2 assimilation rate	nmol $CO_2\,g^{-1}$ (leaf) s^{-1}
A_d	Avg. daily max photosynthesis as fraction of A_{max}	(no units)
K_F	Foliar maintenance respiration as fraction of A_{max}	(no units)
T_{min}	Minimum temperature for photosynthesis	°C
T_{opt}	Optimum temperature for photosynthesis	°C
K_{VPD}	Slope of VPD–photosynthesis relationship	kPa^{-1}
$PAR_{1/2}$	Half saturation point of PAR–photosynthesis relationship	Einsteins m^{-2} day^{-1}
k	Canopy PAR extinction coefficient	(no units)
D_{on}	Day of year for leaf out	day of year
D_{off}	Day of year for leaf drop	day of year
L_{max}	Maximum leaf area index obtained	m^2 (leaf) m^{-2} (ground)
Respiration parameters		
K_A	Wood respiration rate at 0 °C	$g\,C\,g^{-1}\,C\,yr^{-1}$
Q_{10_V}	Vegetation respiration Q_{10}	(no units)
K_H	Soil respiration rate at 0 °C and moisture-saturated soil	$g\,C\,g^{-1}\,C\,yr^{-1}$
Q_{10_S}	Soil respiration Q_{10}	(no units)
Moisture parameters		
f	Fraction of soil water removable in 1 day	(no units)
K_{WUE}	VPD–WUE relationship	mg CO_2 $kPa\,g^{-1}$ H_2O
W_c	Soil water holding capacity	cm (precipitation equivalent)
Tree physiological parameters		
SLW	Density of leaves	$g\,m^{-2}$
C_{frac}	Fractional C content of leaves	$g\,C\,g^{-1}$
K_W	Turnover rate of plant wood C	$g\,C\,g^{-1}\,C\,yr^{-1}$

One additional parameter, T_{max}, the maximum temperature for photosynthesis, was calculated by assuming a symmetric function around the optimum photosynthetic temperature, T_{opt}. That is, for any values of T_{opt} and T_{min}, $T_{max} = T_{opt} + (T_{opt} - T_{min})$.
SIPNET, simplified PnET model; VPD, vapor pressure deficit; PAR, photosynthetically active radiation; WUE, water use efficiency; SLW, specific leaf weight.

positive NEE denotes a net transfer of CO_2 to the atmosphere. These three fluxes are modeled as functions of model state, climate and parameter values. There are a total of 25 parameters and initial conditions that govern the model's behavior, of which, 23 were allowed to vary in the parameter optimization (Tables 1 and 2). A complete description of the equations used in SIPNET is given in Appendix A.

Assimilation scheme

The method that we used to assimilate eddy flux measurements with the SIPNET model can be thought of as an extension of ordinary maximum likelihood parameter optimization. In these procedures, model parameters are iteratively adjusted to yield the best match between data and model. Our data assimilation scheme is based on the Metropolis algorithm (Metropolis *et al.*, 1953). This algorithm performs a quasi-random walk through the parameter space to find the most probable region, defined in terms of the agreement between model and data. The theory of Markov chains (MCs) states that after a sufficient number of steps, each newly generated set of parameter values represents a draw from a stationary distribution. The Metropolis algorithm is constructed in such a way that the stationary distribution is in fact the posterior distribution of the parameters. In each iteration, the algorithm uses the current point to randomly generate a new 'proposal' point in parameter space. It then evaluates the ratio of the posterior probability densities at the new point and the current point: $R = P(\text{new}|\text{data})/P(\text{current}|\text{data})$, where $P(\text{new}|\text{data})$ is the probability that the new proposal point is the

13652486, 2005, 2, Downloaded from https://onlinelibrary.wiley.com/doi/10.1111/j.1365-2486.2005.00897.x by University Of Arizona Library, Wiley Online Library on [24/07/2024]. See the Terms and Conditions (https://onlinelibrary.wiley.com/terms-and-conditions) on Wiley Online Library for rules of use; OA articles are governed by the applicable Creative Commons License

correct parameter set, given the data, and similarly for $P(\text{current}|\text{data})$. If $R>1$ then the algorithm accepts the new point, which then becomes the current point. If $R<1$ then the algorithm accepts the new point with probability equal to R, and rejects it with probability equal to $(1-R)$. If the new point is rejected, then the algorithm takes another random step, again using the current point.

The expressions $P(\text{new}|\text{data})$ or $P(\text{current}|\text{data})$ are in effect the posterior distributions, and according to Bayes' theorem,

$$P(\text{parameter}|\text{data}) \propto L(\text{data})\, P(\text{parameter}), \qquad (2)$$

where $L(\cdot)$ denotes the likelihood function. We assume that the measured NEE values differ from the model predicted values according to a mean zero Gaussian error model, resulting in the likelihood function

$$L = \prod_{i=1}^{n} \frac{1}{\sqrt{2\pi}\sigma} \mathrm{e}^{-(x_i-\mu_i)^2/2\sigma^2}, \qquad (3)$$

where n is the number of half-daily data points, x_i and μ_i are the measured and modeled NEE values respectively (in $\mathrm{g\,C\,m^{-2}}$ summed over a single time step), and σ is the standard deviation on each data point. Note that we assume that each data point has the same standard deviation and that the deviations from the model predictions are independent over time. In principle, different values could be used for σ for each data point. However, since we lacked the information necessary to determine how σ varies with the number of hours contained in each data point and with the current meteorological conditions, we assumed a fixed σ. In practice we used the 'log-likelihood', $\log(L)$, rather than the likelihood, since it is computationally easier to work with. $\mathrm{Log}(L)$ is a negative multiple of the sum-of-squares error statistic that is commonly minimized in least squares estimation (e.g. Bishop, 1995).

If the standard deviations of the data points were known, those values could be used for σ. In this analysis, however, we estimated σ for the Harvard Forest data in each step of the Metropolis algorithm (Hurtt & Armstrong, 1996). For a given point in the parameter space, and thus a given set of μ_i values, it is straightforward to find the value of σ that maximizes $\log(L)$, which we will denote by

$$\sigma_{\mathrm{e}} = \sqrt{\frac{1}{n}\sum_{i=1}^{n}(x_i-\mu_i)^2}. \qquad (4)$$

We then used σ_{e} in place of σ in the calculation of $\log(L)$. Thus in our data assimilation study, σ was treated as a nuisance parameter for which only a single estimate was obtained. As an alternative, σ could be treated as one of the model parameters and be included in the Metropolis algorithm, in which case direct sampling from the posterior of σ is possible (Gelman *et al.*, 1995).

Wherever possible, we used reported values from the literature to set the *a priori* means for each parameter and initial condition (Table 2). Because we did not have detailed information on the uncertainty of each parameter, we specified bounded uniform prior distributions for all parameters (Table 2). For some parameters, the width of the allowable range was based on uncertainty values given by Radtke *et al.* (2001). However, many bounds were based on conventional knowledge of the possible values of each parameter, and from considering the range of values used in other ecosystem models.

Convergence of the Metropolis algorithm to the stationary posterior parameter distribution is guaranteed, but can be slow in high-dimensional parameter problems due to slow mixing, which is the situation of a high rate of rejection of the proposal values of some of the parameters. Optimal acceptance rates are considered to be between 30% and 50%. In order to shorten the burn-in period, we applied a modification that results in an adaptive proposal value at each step in the Metropolis algorithm. The adaptive step helps ensure that the algorithm does not initially get stuck exploring local optima (Hurtt & Armstrong, 1996).

The adaptive algorithm during the initial transient period is based on varying a value, t, for each parameter, that governs the fraction of the parameter's range that can be searched in a single iteration of the optimization. The t values are initially set to 0.5 for each parameter. In each iteration, a parameter i is selected to change, and a random number r is selected between $\pm 0.5t_i$. The proposal parameter value is then generated by

$$p_{\mathrm{new}} = p_{\mathrm{old}} + r(\max - \min), \qquad (5)$$

where p_{old} is the old value of parameter i, p_{new} is the new value of the parameter, and max and min specify the prior range of the given parameter. If p_{new} is outside the parameter's allowable range then a new r is generated and a new p_{new} calculated; this is repeated until an appropriate p_{new} is found. The acceptance criterion is the same as in the standard Metropolis algorithm. If the new point is accepted then t_i is increased by a factor of 1.01. If it is rejected, then t_i is decreased by a factor of 0.99. By changing the t values in this way, they are adjusted until varying any parameter leads to acceptance about 50% of the time.

One of the advantages of the Metropolis algorithm is that it provides complete information about the posterior distributions of the parameters, which can be used to generate standard errors and confidence intervals for individual parameters as well as correlations between

13652486, 2005, 2, Downloaded from https://onlinelibrary.wiley.com/doi/10.1111/j.1365-2486.2005.00897.x by University Of Arizona Library, Wiley Online Library on [24/07/2024]. See the Terms and Conditions (https://onlinelibrary.wiley.com/terms-and-conditions) on Wiley Online Library for rules of use; OA articles are governed by the applicable Creative Commons License

Table 2 Initial SIPNET parameter values and ranges

Parameter	Initial Guess	Source	Range
Initial pool values			
$C_{W,0}$	$11000\,g\,m^{-2}$	Aber *et al.* (1993)	8000–14000
$C_{L,0}$	$0\,g\,m^{-2}$	(Assume no leaves at start)	(Fixed)
$C_{S,0}$	$6300\,g\,m^{-2}$	Magill *et al.* (2000)	3300–9300
W_0	12.0 cm	(Assume $W_0 = W_c$)	(Fixed)
Photosynthesis parameters			
A_{max}	$112\,nmol\,g^{-1}\,s^{-1}$	Aber *et al.* (1996)	91–133
A_d	0.76	Aber *et al.* (1996)	0.66–0.86
K_F	0.1	Aber *et al.* (1996)	0.05–0.2
T_{min}	4.0 °C	Aber *et al.* (1996)	−2.0–10.0
T_{opt}	24.0 °C	Aber *et al.* (1996)	18.0–30.0
K_{VPD}	$0.05\,kPa^{-1}$	Aber *et al.* (1996)	0.01–0.25
$PAR_{1/2}$	$17.0\,E\,m^{-2}\,day^{-1}$	Aber *et al.* (1996)	7.0–27.0
k	0.58	Aber *et al.* (1996)	0.46–0.70
D_{on}	144 (May 24)	(Inspection of data)	91–181
D_{off}	285 (Oct. 12)	(Inspection of data)	243–319
L_{max}	$4.0\,m^{-2}\,m^{-2}$	Barford *et al.* (2001a)	2.0–6.0
Respiration parameters			
K_A	$0.006\,g\,g^{-1}\,yr^{-1}$	Edwards & Hanson (1996)	0.0006–0.06
Q_{10_v}	2.0	(Canonical value)	1.4–2.6
K_H	$0.03\,g\,g^{-1}\,yr^{-1}$	Raich *et al.* (1991) and Aber *et al.* (1997)	0.006–0.15
Q_{10_s}	2.0	(Canonical value)	1.4–2.6
Moisture parameters			
f	0.04	Aber *et al.* (1995)	0.02–0.08
K_{WUE}	$10.9\,mg\,kPa\,g^{-1}$	Aber *et al.* (1995)	7.9–13.9
W_c	12.0 cm	Aber *et al.* (1995)	4.0–36.0
Tree physiological parameters			
SLW	$70.0\,g\,m^{-2}$	S.V. Ollinger (2002), personal communication	50.0–90.0
C_{frac}	$0.45\,g\,g^{-1}$	Aber *et al.* (1995)	0.40–0.50
K_W	$0.03\,g\,g^{-1}\,yr^{-1}$	Aber *et al.* (1995), Barford *et al.* (2001b), and Curtis *et al.* (2002)	0.003–0.3

SIPNET, simplified PnET model; VPD, vapor pressure deficit; PAR, photosynthetically active radiation; WUE, water use efficiency; SLW, specific leaf weight.

parameters. The parameter distributions can be visualized by plotting histograms of the accepted points after the burn-in period.

The method of generating statistics on parameter posterior distributions is valid only after the MC of parameter values has converged to its stationary distribution. We delineate this burn-in period using two criteria. The initial burn-in consists of the adaptive Metropolis phase, with varying parameter t values. We allow this phase to run until the long-term acceptance rates settle within $\pm 2.5\%$ of 50%. After the acceptance rate converges, the algorithm is allowed to run for an additional 5 00 000 iterations while the t values are kept constant. The burn-in period continues, however, until the running means and standard deviations of each parameter have stabilized. In initial tests, it appeared that the means and standard deviations of most parameters had stabilized after the first 1 00 000 points generated with fixed t values. Thus, in computing statistics, we first exclude the points generated before the acceptance rate converges and then exclude the first 20% of the remaining accepted points.

Parameter optimization on synthetic data sets

To determine the expected accuracy of this parameter optimization method applied to SIPNET, we performed a set of runs using a synthetic data set. The 'data' used in these runs were the output of a single model run performed using prescribed parameter values. To

13652486, 2005, 2, Downloaded from https://onlinelibrary.wiley.com/doi/10.1111/j.1365-2486.2005.00897.x by University Of Arizona Library, Wiley Online Library on [24/07/2024]. See the Terms and Conditions (https://onlinelibrary.wiley.com/terms-and-conditions) on Wiley Online Library for rules of use; OA articles are governed by the applicable Creative Commons License

generate this synthetic data set, we arbitrarily fixed each parameter at the mean of the parameter's initial guess value and the lower bound of its prior range (Table 2). Three synthetic data sets were created: one in which the model output was used unchanged, and two in which a normally distributed random 'error' was added to each data point. These random errors had a mean of zero in both cases; their standard deviation was $0.5\,\mathrm{g\,C\,m^{-2}}$ in one data set and $1.0\,\mathrm{g\,C\,m^{-2}}$ in the other. One parameter optimization run was performed using each of these data sets and the retrieved parameter values were compared with the values used to generate the data.

These optimizations can be thought of as sensitivity analyses of the model, in that they provide information about the leverage of NEE data on each model parameter. A multivariate sensitivity analysis like this is an alternative to the standard one-parameter-at-a-time sensitivity analyses that are often performed on models.

Time scale analysis

In order to evaluate the model performance on multiple time scales, we performed a wavelet transformation of the model results, observations and residual (model minus observations) time series (Graps, 1995; Lau & Weng, 1995). The wavelet transform decomposes the time series into multiple time-varying components, and reveals patterns in the data at each scale. This process is similar to Fourier-type frequency band pass filtering but does not require the time series to be stationary. This distinction is important because aggregating the time series to a half-daily time step renders it highly nonstationary.

We used the MATLAB wavelet toolkit and performed a wavelet transformation using the Coif level 5 wavelet basis. The Coif is a standard mother wavelet and was selected because its form is symmetrical and so preserves the characteristic shape of the diurnal and seasonal cycles. The scale and frequency-dependent wavelet coefficients (which operate on the mother wavelet) provide an estimate of the magnitude and timing of variability at each scale evaluated. We evaluated the continuous wavelet transform on the three time series at 100 individual time scales ranging logarithmically from one time step (half-daily) to 7307 time steps (10 years) and computed the variance of the wavelet coefficients at each of those scales.

Results

Initial guess parameter values

The output of the model run with the initial guess parameter values matches the general trends of the data fairly well except that it misses the mid-summer peak CO_2 uptakes apparent in the data (Fig. 2). In addition, there is less wintertime variability in the model output than in the data; it is unclear whether this is due more to data error or to model error. There is a near-perfect fit in the timing of the period of net carbon uptake. This is not surprising since the D_{on} and D_{off} parameters were adjusted to fit the data. The sizes of both the vegetation and soil carbon pools increase slightly over the 10-year model run (Fig. 3a), as would be expected for an aggrading forest (Barford *et al.*, 2001b).

The root mean squared (RMS) error of this run was $1.37\,\mathrm{g\,C\,m^{-2}}$ (this and subsequent errors are expressed as flux over a single time step, unless stated otherwise). The total modeled NEE over the 10 years was approximately half the uptake indicated by the data. Although there are a few years in which the two interannual variability patterns were similar, there was little overall correlation between the model and data interannual variability. The mean absolute error in these interannual variability estimates was $57.2\,\mathrm{g\,C\,m^{-2}\,yr^{-1}}$.

Optimization results

To test the optimization algorithm, we performed five optimization runs, each using different random number seeds to determine the successive Metropolis steps, and compared the retrieved parameter means and standard deviations from each. There are only two parameters for which the retrieved values differed by more than one standard deviation from one run to another: A_{max}

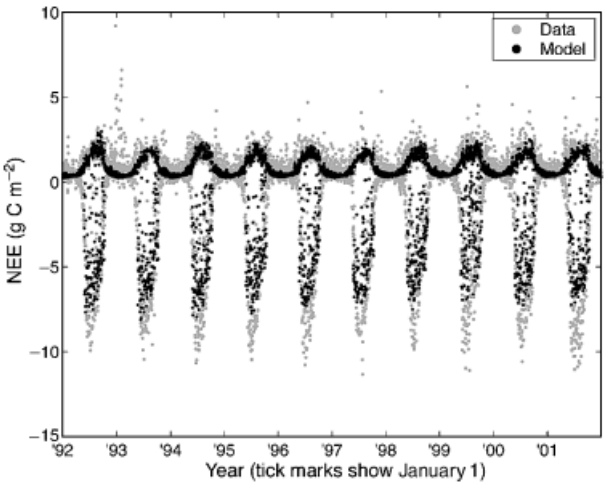

Fig. 2 Comparison of data with output of model run with initial guess parameter values. Each point represents the data or model output for a single half-daily time step. Positive net ecosystem exchange of CO_2 (NEE) corresponds to a net loss of CO_2 from the terrestrial ecosystem to the atmosphere.

13652486, 2005, 2, Downloaded from https://onlinelibrary.wiley.com/doi/10.1111/j.1365-2486.2005.00897.x by University Of Arizona Library, Wiley Online Library on [24/07/2024]. See the Terms and Conditions (https://onlinelibrary.wiley.com/terms-and-conditions) on Wiley Online Library for rules of use; OA articles are governed by the applicable Creative Commons License

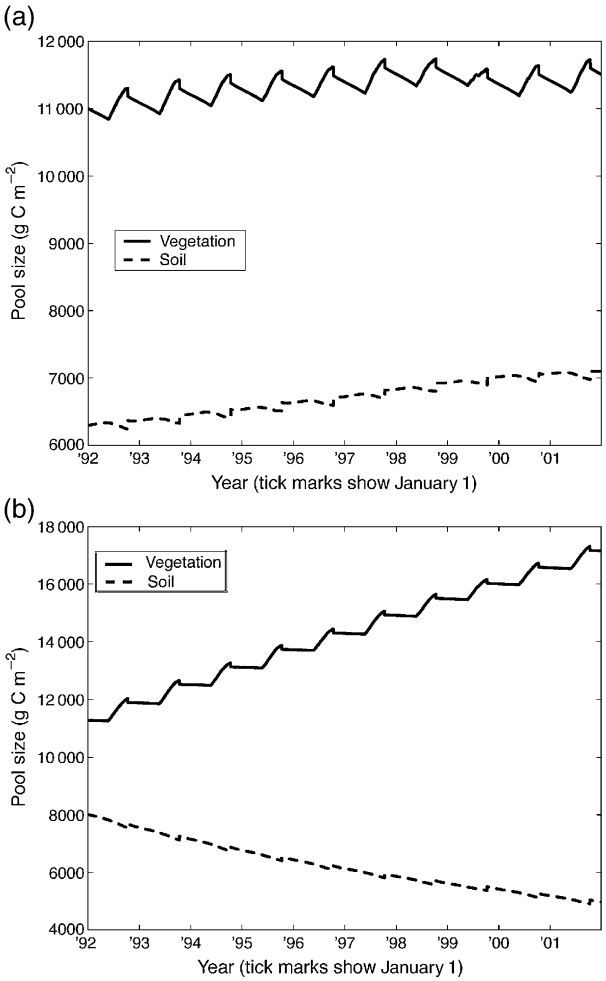

Fig. 3 (a) Dynamics of model run with initial guess parameter values. (b) Dynamics of model run with best parameter set retrieved from parameter optimization. The vegetation pool is the sum of plant wood carbon and plant leaf carbon.

and specific leaf weight (SLW). Furthermore, the log likelihoods of the best points found in each of these runs differed by less than one log likelihood point, indicating that the algorithm was always converging at or near the global optimum. Because of the general similarity of these five runs, the remaining analyses were performed using only a single run (Table 3).

Means and standard deviations alone do not provide complete information about the retrieved parameters. Additional insight can be gained by examining the histograms of the retrieved values (Fig. 4). These histograms show what will be referred to as 'parameter behavior'. The parameter behaviors generally fell into one of three categories: 'well-constrained', 'poorly constrained', or 'edge-hitting'.

Well-constrained parameters exhibited a well-defined unimodal distribution. The range of retrieved parameters could either be a small fraction of the prior allowable range (as for T_{min}, Fig. 4a) or a large fraction of the range (as for K_F, Fig. 4b), but in general well-constrained parameters tended to have small retrieved standard deviations relative to the parameters' allowable ranges. Most parameters fell into this category (Table 3).

Table 3 Means and standard deviations of retrieved parameters for the base case

Parameter	Posterior value	Parameter class
Best LL*	−5140.8	NA
Mean LL*	−5151.1 ± 3.3	NA
Mean σ_e†	0.974 ± 0.001	NA
$C_{W,0}$	10505 ± 1555	Poorly constrained
$C_{S,0}$	6229 ± 1314	Well-constrained
A_{max}	118.3 ± 11.3	Well-constrained
A_d	0.744 ± 0.044	Well-constrained
K_F	0.162 ± 0.019	Well-constrained
T_{min}	1.46 ± 0.44	Well-constrained
T_{opt}	28.9 ± 0.7	Edge-hitting
K_{VPD}	0.138 ± 0.008	Well-constrained
$PAR_{1/2}$	7.53 ± 0.41	Edge-hitting
k	0.586 ± 0.065	Poorly constrained
D_{on}	143.1 ± 0.3	Well-constrained
D_{off}	284.0 ± 0.8	Well-constrained
L_{max}	4.44 ± 0.58	Well-constrained
K_A	.0022 ± .0015	Edge-hitting
Q_{10_V}	1.62 ± 0.10	Well-constrained
K_H	0.080 ± 0.018	Well-constrained
Q_{10_S}	1.42 ± 0.02	Edge-hitting
f	0.046 ± 0.011	Well-constrained
K_{WUE}	13.0 ± 0.6	Edge-hitting
W_c	21.9 ± 4.0	Well-constrained
SLW	55.6 ± 3.8	Edge-hitting
C_{frac}	0.452 ± 0.026	Poorly constrained
K_W	0.010 ± 0.004	Edge-hitting

*LL = Log likelihood. Larger values (*i.e.*, closer to zero) indicate greater likelihood.

†σ_e = Estimated data standard deviation (g C m^{-2} over a single time step). This value represents a combination of data error and process representation error, and is equivalent to the model-data RMS error.

After convergence to a stationary distribution, approximately 400 000 Metropolis steps and likelihood calculations were performed. These values were repeatable (differences less than one standard deviation) in four additional estimations using different random number seeds to determine the successive Metropolis steps, except A_{max} and SLW, which varied by less than 10%. Parameter class indicates the behavior of the estimated posterior distributions (see text). For comparison, the log likelihood of the unoptimized model was −6407.8, with an RMS error of 1.37 g C m^{-2}. VPD, vapor pressure deficit; PAR, photosynthetically active radiation; WUE, water use efficiency; SLW, specific leaf weight; NA, not applicable.

13652486, 2005, 2, Downloaded from https://onlinelibrary.wiley.com/doi/10.1111/j.1365-2486.2005.00897.x by University Of Arizona Library, Wiley Online Library on [24/07/2024]. See the Terms and Conditions (https://onlinelibrary.wiley.com/terms-and-conditions) on Wiley Online Library for rules of use; OA articles are governed by the applicable Creative Commons License

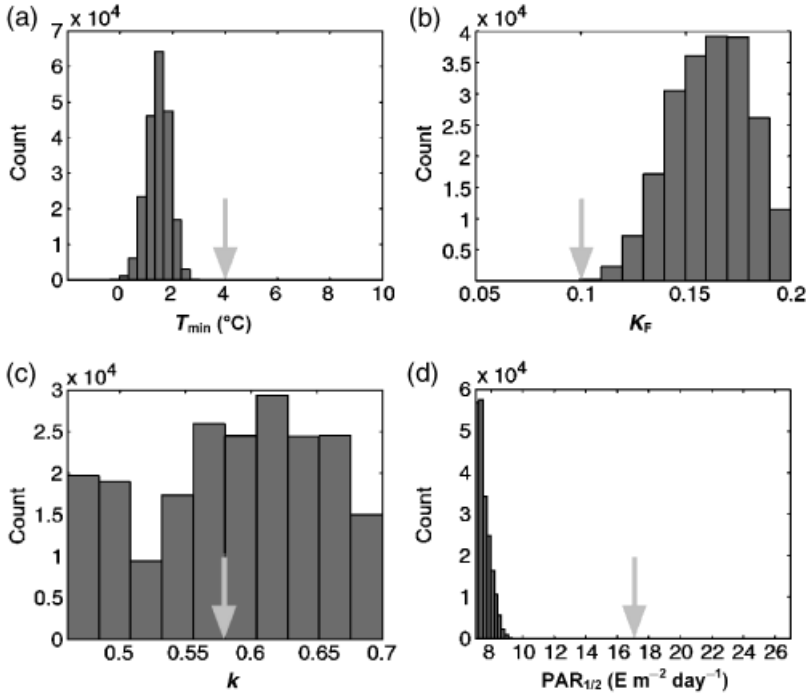

Fig. 4 Results from the Bayesian parameter estimation exercise, using a simplified ecosystem model and CO_2 flux data. Histograms show posterior estimates of parameters that govern net ecosystem exchange of CO_2. The arrows indicate the prior mean values, and the ranges of the i-axes indicate the ranges of the parameters' prior uniform distributions. PAR, photosynthetically active radiation.

Poorly constrained parameter distributions were relatively flat, with large standard deviations, (e.g. *k*) (Fig. 4c). Three parameters were poorly constrained (Table 3).

Edge-hitting parameters were those for which the mode of their retrieved values occurred near one of the edges of their allowable range, and most of the retrieved values were clustered near this edge (such as $PAR_{1/2}$, Fig. 4d). For these parameters, it appears that widening the range on the edge-hit side would cause the retrieved parameter mean to be shifted in that direction. There were seven edge-hitting parameters (Table 3).

By definition, the half-daily NEE predicted by the model with optimized parameter values matched the data more closely than the values predicted using initial guess parameter values (Fig. 5). The best point found had an RMS error of $0.972\,g\,C\,m^{-2}$, a significant improvement over the model run with initial guess parameter values. The most noticeable difference between the run with optimized parameter values and that with initial guess values is that the optimized model had greater summer daytime uptake of CO_2, following the pattern seen in the data. Note, however, that there was still less wintertime variability in the model output than in the data, as can be seen from the cloud of points where the model predicts a relatively constant NEE of about $1\,g\,C\,m^{-2}$, while the measurements show considerably more variability (Fig. 5).

There was also a large improvement in the estimation of total NEE over the ten year period. Interannual timescale adjustments, however, were more subtle. The model, postassimilation, matched the data's interannual variability only slightly better than the first guess, with a mean absolute error in interannual variability of $49.2 \pm 6.3\,g\,C\,m^{-2}\,yr^{-1}$ (where the uncertainty indicates one standard deviation across all parameter sets retrieved from the optimization; subsequent uncertainty values will also be expressed as one standard deviation).

On the decadal time scale, the model's dynamics were unrealistic, with the vegetation carbon pool growing dramatically and the soil carbon pool falling by a similar amount (Fig. 3b). Results of performing a separate parameter optimization for each year of data suggest that these unrealistic dynamics may arise because the optimal partitioning of ecosystem respiration into heterotrophic and autotrophic respiration varies on an interannual time scale. There were large differences in the retrieved values of the vegetation and soil respiration rate parameters from one year to another (Table 4). Moreover, there was a generally increasing trend in vegetation respiration rate with time (best linear fit: $0.0018\,(g\,g^{-1}\,yr^{-1})\,yr^{-1}$, $R^2 = .313$), and a generally decreasing trend in soil respiration rate (best linear fit: $-0.0043\,(g\,g^{-1}\,yr^{-1})\,yr^{-1}$, $R^2 = .416$). With the respiration rate constants held fixed over time, the only

13652486, 2005, 2, Downloaded from https://onlinelibrary.wiley.com/doi/10.1111/j.1365-2486.2005.00897.x by University Of Arizona Library, Wiley Online Library on [24/07/2024]. See the Terms and Conditions (https://onlinelibrary.wiley.com/terms-and-conditions) on Wiley Online Library for rules of use; OA articles are governed by the applicable Creative Commons License

way the model can achieve these changes in respiration partitioning is through changes in the vegetation and soil carbon pool sizes. The relative growth of the vegetation pool and relative decline of the soil pool in the 10-year optimizations had a similar effect to the changes in the rate constants in the 1-year optimizations. This unrealistic result could also reflect a structural error in the model, such as the lack of interannual variability in allocation to roots. Although fine root dynamics are either ignored or oversimplified in many ecosystem models, they are responsible for much of the temporal variability in total soil respiration (Ryan & Law, in press). We chose not to attempt a better fit in the absence of a clear *a priori* hypothesis and mechanism because of the danger of obtaining a spuriously improved result through overfitting.

The use of a Bayesian approach to parameter optimization allows the generation of confidence intervals on the model's predictions. The distributions obtained by running the model forward on each parameter set retrieved from the parameter estimation represent posterior estimates of NEE for each time step, conditioned on the observed fluxes, the model equations, and the parameter priors (Fig. 6). Although there were large uncertainties in some of the retrieved parameters (Table 3), the uncertainty in the model's predicted NEE was relatively small for most time steps. This indicates that either the parameter uncertainties tended to cancel through correlations between parameters (Fig. 7), or the parameters with large uncertainties had little effect on the model's NEE predictions, or, most likely, some combination of the two. The two times of year when there were large uncertainties in the predicted NEE were at the start and end of the growing season. Because SIPNET uses a step function for leaf growth and senescence, small differences in the parameters governing the dates of these events lead to large differences in predicted NEE around these times. The effect of this step function can also be seen in the pattern of model-data residuals (Fig. 6c, d). The model predicts too little carbon uptake just before the date of leaf growth and too much just after this date; a similar pattern occurs in the fall. These plots also suggest that the constant variance assumption in the likelihood (Eqn. (3)) may not be realistic and perhaps separate likelihood models should be considered that account for changing seasonal error variability.

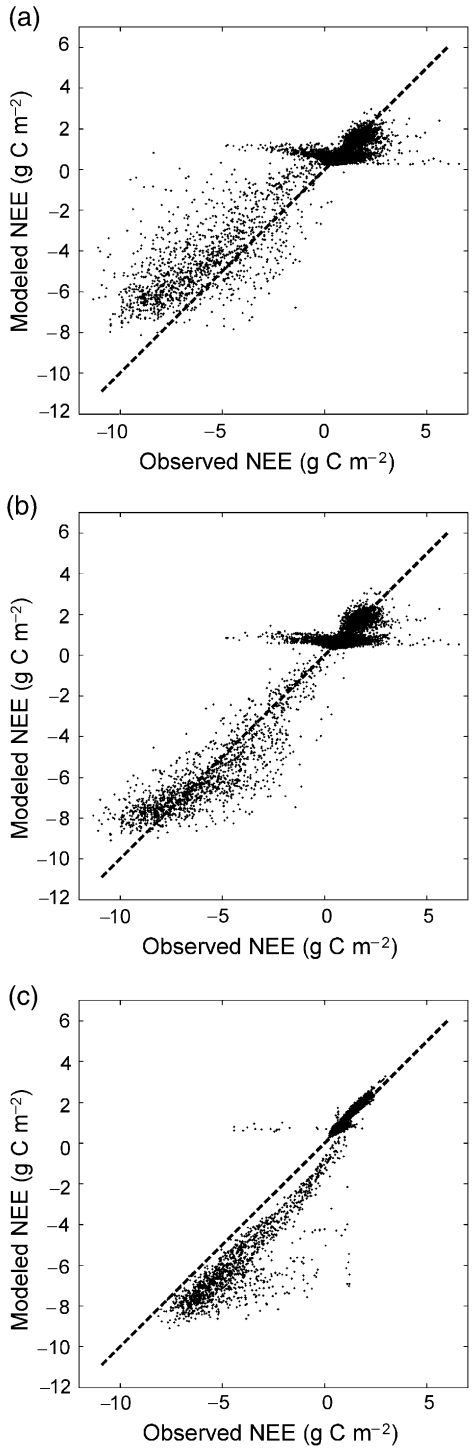

Fig. 5 (a) Modeled vs. observed net ecosystem exchange of CO_2 (NEE) using initial best-guess parameters, (b) modeled vs. observed NEE using optimized parameters, (c) the two model results against one another, showing how the observations constrained the realized parameter values. Note that improvements in uptake estimates are larger than for respiration and that the initial guess misses the high summertime uptake flux and so greatly underestimates the annual total. The model suggests less variability in winter respiration fluxes than the observations, even after parameter optimization.

13652486, 2005, 2, Downloaded from https://onlinelibrary.wiley.com/doi/10.1111/j.1365-2486.2005.00897.x by University Of Arizona Library, Wiley Online Library on [24/07/2024]. See the Terms and Conditions (https://onlinelibrary.wiley.com/terms-and-conditions) on Wiley Online Library for rules of use; OA articles are governed by the applicable Creative Commons License

Table 4 Means and standard deviations of vegetation and soil respiration rate parameters retrieved from performing a separate parameter optimization on each year of data

	1992	1993	1994	1995	1996	1997	1998	1999	2000	2001
K_A	.0076 ± .0061	.0044 ± .0045	.0118 ± .0092	.0047 ± .0037	.0158 ± .0090	.0037 ± .0032	.0142 ± .0077	.0033 ± .0026	.0146 ± .0081	.0362 ± .0065
K_H	.0436 ± .0112	.0905 ± .0128	.0429 ± .0150	.0407 ± .0074	.0352 ± .0136	.0586 ± .0077	.0285 ± .0118	.0351 ± .0075	.0322 ± .0121	.0153 ± .0083
Ratio of means (K_A/K_H)	0.174	0.049	0.276	0.115	0.448	0.062	0.499	0.093	0.454	2.363

All optimizations had $C_{W,0}$ fixed at 11000 g m^{-2} and $C_{S,0}$ fixed at 6300 g m^{-2}. Linear regressions between mean retrieved parameter values and year give a slope of 0.0018 (g g^{-1} yr^{-1}) yr^{-1} for K_A (base wood respiration rate; R^2 = .313) and a slope of −0.0043 (g g^{-1} yr^{-1}) yr^{-1} for K_H (base soil respiration rate; R^2 = .416).

Synthetic data sets

The results of performing the parameter optimization on three synthetic data sets with varying amounts of added noise are shown in Table 5. The estimated values for the standard deviation of the data (σ_e) matched the values used to generate the data sets almost exactly. This close match suggests that this optimization method can be used to estimate the uncertainty on a data set, relative to a given model, when this uncertainty is unknown, assuming the error is normally distributed. The most useful results are those obtained using the data set with $\sigma = 1.0\,\mathrm{g\,C\,m^{-2}}$ since this value for σ is close to that retrieved for the actual data set ($\sigma_e = 0.974 \pm 0.001\,\mathrm{g\,C\,m^{-2}}$) (Table 3).

Parameters whose posterior means were within $0.5 \times (\mathit{InitialGuess} - \mathit{Actual})$ of *Actual* (where *Actual* is the actual parameter value used to generate the synthetic data set) are shown in bold in Table 5. This metric can be used to determine which parameters the optimization is able to estimate well. The number of parameters satisfying this criterion decreased only slightly with increasing data error: 17 parameters with no error, 16 with $\sigma = 0.5\,\mathrm{g\,C\,m^{-2}}$ and 15 with $\sigma = 1.0\,\mathrm{g\,C\,m^{-2}}$.

In general, the retrieved parameter uncertainties (i.e. the standard deviation of the posterior parameter distributions), were larger for the data sets with greater added noise. With more data error, a wider range of parameter values could yield approximately equally good model-data fits.

Discussion

Overall performance of the parameter optimization

Parameter optimization reduced the model-data RMS error by 29%, from 1.37 g C m^{-2} (initial) to 0.972 g C m^{-2} (optimized). Both values, however, are relatively large in comparison to the mean magnitude of the half-daily data, 1.91 g C m^{-2}. The error using the initial guess values is due to a combination of three factors: errors in the model structure, data errors and parameter errors. The parameter optimization can decrease only the last of these three sources of error. The similarity of the log likelihood estimates of the best points found in each of the base runs suggests that the optimization is indeed finding the best possible points in the parameter space, conditioned on the choice of model. Results from the optimizations performed using synthetic data sets further suggest that this algorithm finds acceptable values for the majority of SIPNET parameters.

To test the robustness of this parameter optimization method, we adjusted three aspects of the methodology that were most likely to affect the results of the MCMC

13652486, 2005, 2, Downloaded from https://onlinelibrary.wiley.com/doi/10.1111/j.1365-2486.2005.00897.x by University Of Arizona Library, Wiley Online Library on [24/07/2024]. See the Terms and Conditions (https://onlinelibrary.wiley.com/terms-and-conditions) on Wiley Online Library for rules of use; OA articles are governed by the applicable Creative Commons License

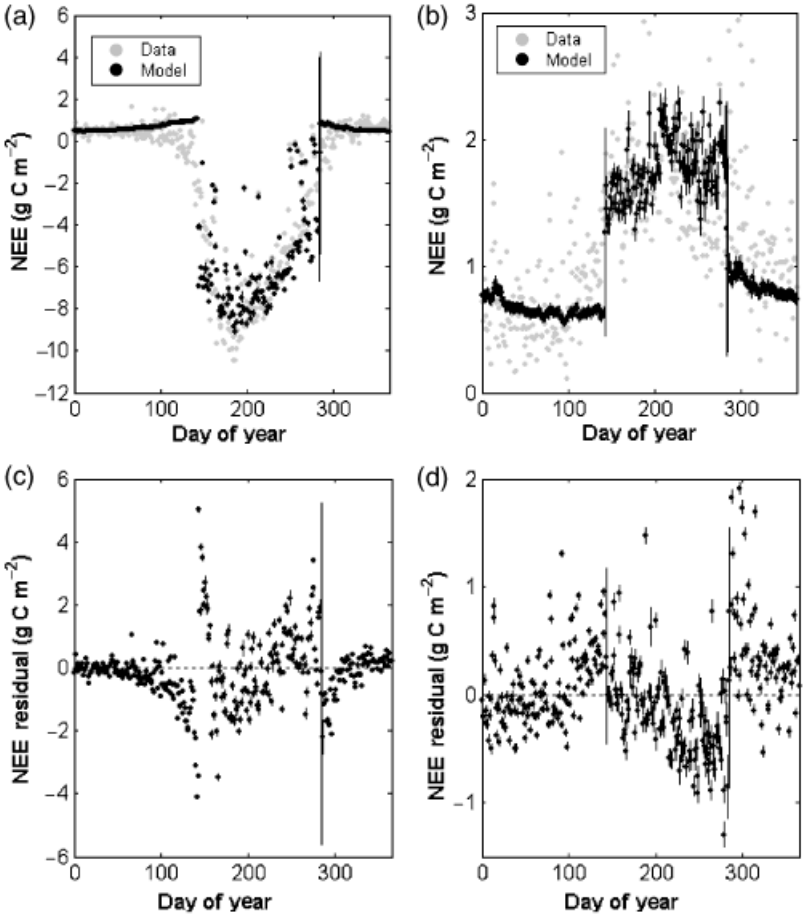

Fig. 6 Confidence intervals on one representative year of posterior net ecosystem exchange of CO_2 (NEE) estimates (1995), plotted against the data. Positive NEE corresponds to a net loss of CO_2 from the terrestrial ecosystem to the atmosphere. (a) Modeled vs. observed daytime NEE, (b) modeled vs. observed nighttime NEE, (c) daytime NEE residuals (data – model), (d) nighttime NEE residuals. Error bars indicate two standard deviations of model predictions. Note that the uncertainty on most NEE predictions is relatively small despite large uncertainty on some model parameters. However, there are some systematic biases in the model relative to the data, following a roughly seasonal pattern (c, d).

optimization. First, we used a different set of parameter values as a starting point for the optimization. Second, we modified the parameters' t values so that each individual Metropolis step would tend to be smaller than in the unmodified algorithm. Third, we applied a stricter filter to the data. Using this stricter filter, a half-daily interval was included in the model-data comparison only if all the hours making up that interval were observed (the unmodified algorithm allowed up to 50% of the hours making up a data point to be gap-filled). This last modification was the only one that led to significant differences in the results of the parameter optimization. Nine of the resulting model parameters differed by more than one standard deviation from their posterior mean using the unmodified algorithm. It remains unclear whether using some gap-filled points or using only measured data yields better results in the parameter optimization, highlighting tradeoffs between gap-filling errors and the effects of missing data.

Parameter uncertainty analysis

Two independent metrics can provide insight into the information content of the data with respect to the different model parameters and processes. First, the accuracies of the parameter values retrieved when optimizing on a synthetic data set indicate how well each model parameter can theoretically be constrained using NEE data alone. Second, the shape of the posterior parameter distributions indicate the degree to which the parameters are constrained, relative to the priors, by the actual observations. An additional consideration is that parameters whose values are highly correlated (Fig. 7)

13652486, 2005, 2, Downloaded from https://onlinelibrary.wiley.com/doi/10.1111/j.1365-2486.2005.00897.x by University Of Arizona Library, Wiley Online Library on [24/07/2024]. See the Terms and Conditions (https://onlinelibrary.wiley.com/terms-and-conditions) on Wiley Online Library for rules of use; OA articles are governed by the applicable Creative Commons License

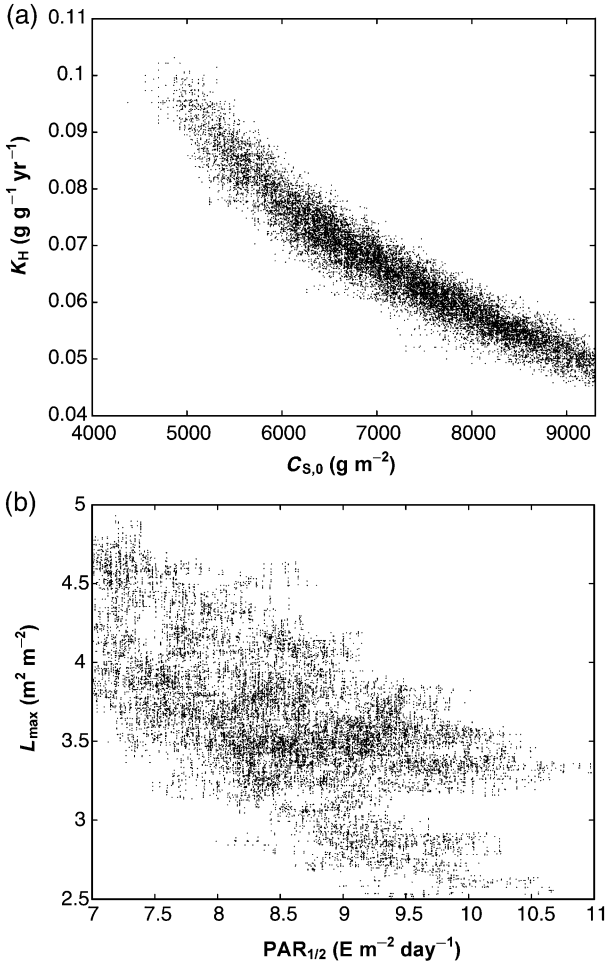

Fig. 7 Two representative pair-wise parameter correlations. Each point on the graph is from one iteration of the parameter optimization on a synthetic data set. This data set was generated using the best parameter set from the base run and had a normally distributed data error with a mean of 0 and a standard deviation of 1.0. Using a synthetic data set allowed a probing of only the model, with data effects excluded. (a) shows a pair of parameters with a correlation coefficient of −0.95, and (b) shows a pair of parameters with a correlation coefficient of −0.62.

are not independently estimated when using NEE as the dependent variable. These include parameters whose product influences the flux.

To some extent, the synthetic optimizations and the parameter distributions yield similar conclusions. $C_{W,0}$, k and C_{frac}, the three parameters that were poorly constrained, were also parameters for which inaccurate estimates were obtained in the optimizations on synthetic data sets. These inaccuracies appeared even when using a data set with no error (Table 5). Either the modeled NEE is insensitive to these parameters, or there are strong correlations between these parameters and others in the model. We expect that the first cause explains the poorly constrained nature of $C_{W,0}$ and C_{frac}, and the second explains the poorly constrained nature of k. We should not expect all parameters to be constrained by a given data set, even if it is necessary to include them in the model. This highlights the value of using a method that allows the incorporation of prior knowledge of ecophysiological parameters.

Most other parameters that were estimated inaccurately in the synthetic optimization also had large retrieved standard deviations in the optimization on the actual data set, despite being categorized as well-constrained (Tables 3 and 5). As with the poorly constrained parameters, the NEE data contain little information about these parameters. One significant exception is K_{VPD}, the slope of the relationship between VPD and photosynthesis. With a low value of K_{VPD}, like that used to generate the synthetic data set, the model seems to be relatively unaffected by small perturbations to this parameter (Table 5). The actual data set, however, contains more information about this parameter and suggests that its value is relatively high (Table 3). For parameters like this one that govern the model's sensitivity to environmental conditions, it is reasonable to expect such a correlation between parameter value and estimation accuracy. If the parameter value is high, the model component using that parameter will have a relatively large influence on modeled NEE and so, conversely, NEE data will have relatively high leverage on that parameter value. If, on the other hand, the parameter value is low, the opposite will hold, and NEE data will have relatively little leverage on that parameter value.

Parameters that were well-constrained by the data and were estimated accurately in the synthetic optimization are those for which the data contain significant information, conditioned on the model equations. D_{on} and D_{off}, for instance, both have a large influence on the model's predicted NEE, and their effects are relatively independent of other model parameters. Consequently these parameters were particularly well-constrained and accurately estimated in the synthetic optimization (Tables 3 and 5).

The data also contain significant information about edge-hitting parameters, although in this case the information in the data conflicts with our prior choice. These conflicts in information, however, can yield insights leading to model or data improvements. Some parameters may have hit the edge because of unmodeled biases in the climate or NEE data. In addition, the half-daily aggregation of data could lead to scale-dependent errors in the retrieved parameters relative to the priors. Some parameters govern processes whose characteristic time scale is on the order of minutes or hours rather than half-days. $PAR_{1/2}$, for

13652486, 2005, 2, Downloaded from https://onlinelibrary.wiley.com/doi/10.1111/j.1365-2486.2005.00897.x by University Of Arizona Library, Wiley Online Library on [24/07/2024]. See the Terms and Conditions (https://onlinelibrary.wiley.com/terms-and-conditions) on Wiley Online Library for rules of use; OA articles are governed by the applicable Creative Commons License

Table 5 Posterior means and standard deviations of estimated parameters from each of the three synthetic runs: no data error, normally distributed data error with standard deviation (σ) of $0.5\,\mathrm{g\,C\,m^{-2}}$, and normally-distributed data error with standard deviation of $1.0\,\mathrm{g\,C\,m^{-2}}$

Parameter	Initial guess	Actual	No error	$\sigma = 0.5$	$\sigma = 1.0$
Mean σ_e*	NA	NA	0.0092 ± 0.0085	0.50 ± 0.0002	1.0 ± 0.0004
$C_{W,0}$	11000	9500	8591 ± 265	10351 ± 1514	10287 ± 1497
$C_{S,0}$	6300	4800	5723 ± 82	6746 ± 1754	6650 ± 1566
A_{max}	112	101.5	110.1 ± 0.3	**101.1 ± 7.6**	**107.2 ± 11.6**
A_d	0.76	0.710	0.675 ± 0.001	0.740 ± 0.053	0.752 ± 0.057
K_F	0.1	0.075	**0.071 ± 0.0003**	**0.074 ± 0.007**	**0.075 ± 0.011**
T_{min}	4.0	1.00	**1.00 ± 0.01**	**1.29 ± 0.34**	**1.51 ± 0.62**
T_{opt}	24.0	21.0	**21.0 ± 0.01**	**20.4 ± 0.3**	**20.0 ± 0.6**
K_{VPD}	0.05	0.030	**0.030 ± 0.001**	0.051 ± 0.027	0.069 ± 0.033
$PAR_{1/2}$	17.0	12.00	**11.79 ± 0.04**	**11.01 ± 0.84**	**13.51 ± 1.60**
k	0.58	0.520	0.551 ± 0.002	0.617 ± 0.060	0.566 ± 0.064
D_{on}	144	117.5	**117.5 ± 0.2**	**117.2 ± 0.3**	**117.2 ± 0.3**
D_{off}	285	264.0	**264.0 ± 0.1**	**264.1 ± 0.3**	**264.3 ± 0.3**
L_{max}	4.0	3.00	**2.93 ± 0.01**	**3.42 ± 0.49**	**2.91 ± 0.57**
K_A	0.006	0.0033	**0.0035 ± 0.0001**	**0.0028 ± 0.0017**	**0.0040 ± 0.0022**
Q_{10v}	2.0	1.70	**1.70 ± 0.003**	**1.74 ± 0.07**	**1.74 ± 0.13**
K_H	0.03	0.018	**0.015 ± 0.0002**	**0.015 ± 0.007**	0.010 ± 0.004
Q_{10s}	2.0	1.70	**1.70 ± 0.005**	**1.58 ± 0.09**	**1.61 ± 0.16**
f	0.04	0.030	**0.031 ± 0.001**	**0.030 ± 0.002**	**0.030 ± 0.003**
K_{WUE}	10.9	9.4	10.2 ± 0.9	**9.3 ± 0.3**	**9.2 ± 0.6**
W_c	12.0	8.0	**7.2 ± 0.7**	**8.2 ± 0.5**	**8.4 ± 0.9**
SLW	70.0	60.0	**59.9 ± 0.1**	**57.1 ± 4.6**	**62.4 ± 8.7**
C_{frac}	0.45	0.425	**0.423 ± 0.025**	0.450 ± 0.026	0.450 ± 0.026
K_W	0.03	0.0165	**0.021 ± 0.001**	0.073 ± 0.084	0.136 ± 0.093

*σ_e = Estimated data standard deviation ($\mathrm{g\,C\,m^{-2}}$ over a single time step). This value represents a combination of data error and process representation error, and is equivalent to the model-data RMS error.

'Initial guess' values represent the starting point for the parameter optimization; these values are the same as the initial guess values used elsewhere. 'Actual' values are the parameter values used to generate the synthetic data set. For each parameter, its 'actual' value is the mean of its initial guess value and the lower bound of its prior range. If the optimization were perfect, the retrieved values would be the same as the actual values. Parameter values shown in bold are those whose retrieved values were within $0.5 \cdot (\mathit{InitialGuess} - \mathit{Actual})$ of *Actual*. VPD, vapor pressure deficit; PAR, photosynthetically active radiation; WUE, water use efficiency; SLW, specific leaf weight; NA, not applicable.

example, governs the change in photosynthetic uptake due to the amount of incoming solar radiation, which changes significantly over a single day, potentially explaining its edge-hitting behavior.

Edge-hitting parameters may also illuminate deficiencies in model structure, indicating lack of realism in the model process that uses that parameter. For example, the high water use efficiency (WUE) (K_{WUE}) suggested by the optimization may indicate that there is less water stress at this site than is predicted by the model equations. Indeed, Aber *et al.* (1995) found that this area of Harvard Forest experiences little or no water stress. Similarly, one possible reason for the low Q_{10s} values, as well as for the lower-than-expected Q_{10v} values, is that SIPNET may be missing or misrepresenting a process that causes net CO_2 uptake to be high at high temperatures; this appears to be the case in graphs of model vs. data NEE (Figs 2, 5). The parameter optimization could be compensating for this by lowering the respiration Q_{10} values, forcing respiration to be lower than it should be when the temperature is high. The unexpectedly high T_{opt} parameter also suggests that SIPNET may be lacking a process that increases CO_2 uptake at higher temperatures. Finally, the extremely low values retrieved for K_A, taken in conjunction with higher-than-expected values for K_F, indicate that there may be a problem in SIPNETs calculation of vegetation respiration. The optimized parameter values force vegetation respiration to be lower in the winter and higher in the summer than it is with the initial guess parameter values. This may indicate a need to disaggregate vegetation respiration, either by splitting it into growth and maintenance respiration or by explicitly modeling fine root respiration.

13652486, 2005, 2, Downloaded from https://onlinelibrary.wiley.com/doi/10.1111/j.1365-2486.2005.00897.x by University Of Arizona Library, Wiley Online Library on [24/07/2024]. See the Terms and Conditions (https://onlinelibrary.wiley.com/terms-and-conditions) on Wiley Online Library for rules of use; OA articles are governed by the applicable Creative Commons License

Of course, some parameters may have hit the edge simply because their prescribed ranges were too narrow. This possibility could be tested by increasing these parameter ranges and re-running the optimization. However, in preliminary experiments we found that it is difficult to do this without forcing other (previously well-constrained) parameters to be edge-hitting. If one parameter is allowed to take on unrealistic values, the model is only able to maintain its close match to the data if other parameters take on unrealistic values as well. Finally, parameters that vary by order of magnitudes (such as K_W) are indicative of multiplicative effects, and typically exhibit a highly skewed (e.g. logarithmic) distribution.

Error analysis and wavelet decomposition

The optimization resulted in significant reduction in overall error on the daily time scale, especially for periods of net uptake (Fig. 5). While the mean reduction in model-data RMS error is only from 1.37 to $0.972\,\mathrm{g\,C\,m^{-2}}$, the improvement in mid-summer maxima is very large, greatly improving the overall estimation of photosynthetic uptake. The greater improvement in summer vs. winter (uptake vs. release) is consistent with other model diagnostics. These results are consistent with an emerging conclusion that greater uncertainties remain in modeling respiration than photosynthesis on these timescales. The model, before and after parameter optimization, predicts much less variability in winter and nighttime respiration fluxes than the observations show; in fact, the observations show some periods of net carbon uptake in the winter. This area of disagreement probably reflects both missing processes in the model and observational uncertainty, although we do not know the exact causes of this disagreement yet. Comparison of modeled fluxes to other respiration (e.g. soil chamber) data will be valuable in diagnosing the causes of these model-data discrepancies.

The wavelet transformation complements the above analysis by visualizing the variance of the model, data, and model-data mismatch at multiple time scales (Fig. 8). The observations show large variance at the strongly forced diurnal and seasonal time scale and an overall correlation between frequency and variance, with variance declining at lower frequencies. This corresponds to the small magnitude of long-term NEE compared to photosynthetic and respiratory fluxes. The variance of the residuals, relative to the variance of the data, indicates the fit at each scale.

The residual variance is low at the strongly forced diurnal and seasonal time scales. The ability of the optimization to fit the data's variability patterns at both of these time scales simultaneously, while using only a single parameter set, indicates the effectiveness of this approach, in which all the data are considered at once. Other methods of parameter estimation often produce different parameter values (e.g. different values for the Q_{10} parameters) for the diurnal and seasonal fits (e.g. Reichstein *et al.*, 2003). However, the residual variance generally increases at low frequencies. The model explains much of the variance in the strongly forced fluxes, but fails to capture interannual patterns of net carbon exchange, which are more heavily influenced by the internal dynamics of the ecosystem. These variance patterns indicate that the bulk of the information in even a decadal eddy covariance record, given the signal to noise of the record, is on the seasonal and shorter time scales.

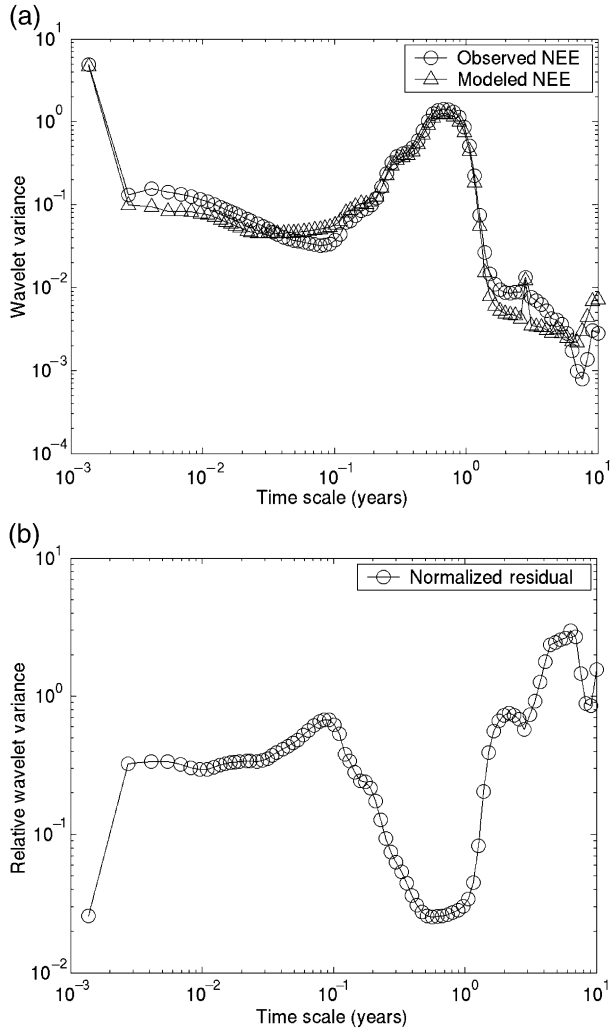

Fig. 8 Wavelet variance of the net ecosystem exchange of CO_2 observations (a) and of the normalized residual (b) (the model-data difference divided by the data).

13652486, 2005, 2, Downloaded from https://onlinelibrary.wiley.com/doi/10.1111/j.1365-2486.2005.00897.x by University Of Arizona Library, Wiley Online Library on [24/07/2024]. See the Terms and Conditions (https://onlinelibrary.wiley.com/terms-and-conditions) on Wiley Online Library for rules of use; OA articles are governed by the applicable Creative Commons License

Table 6 Error statistics from optimizations on the unmodified model and two runs testing modifications of the model structure, in which interannual variability was introduced into the timing of leaf growth

	Unmodified model	10 D_{on} parameters	GDD-based leaf out
Best LL*	−5140.8	−5008.2	−5180.7
Mean LL*	−5151.1 ± 3.3	−5019.5 ± 3.8	−5189.8 ± 3.2
Mean σ_e†	0.974 ± 0.001	0.940 ± 0.001	0.985 ± 0.001
IV error‡	49.2 ± 6.3	58.0 ± 6.6	55.6 ± 4.4

*LL = Log Likelihood. Larger (i.e. closer to zero) numbers mean greater likelihood.
†σ_e = Estimated data standard deviation (g C m^{-2} over a single time step). This value represents a combination of data error and process representation error, and is equivalent to the model-data RMS error.
‡IV error = Mean absolute error in interannual variabilities between model and data in g C m^{-2} yr^{-1}.
For the '10 D_{on} parameters' run, the single D_{on} parameter was replaced by 10 such parameters, one for each year, each optimized independently. For the 'GDD-based leaf out' run, leaf growth was determined by the accumulation of GDDs rather than by a fixed date. GDD, growing degree-day.

Wavelet decomposition is useful for analyzing flux data because the correlation between frequency and variance tends to mask many of the slow processes (Torrence & Compo, 1998). The low frequency variations are nearly an order of magnitude smaller than the amplitudes of the highest frequencies (Fig. 8). Although the model does not simulate the timing of the slower processes very well, the observations and model do show similar amplitude-frequency correlations across the wavelet spectrum. The amplitude of signals related to interannual and long-term NEE are very small relative to diurnal, synoptic and seasonal changes. Most parameter estimation approaches are more sensitive to the larger amplitude changes, especially relative to the assumed error of the measurement. Partitioning the signal into time-scales allows careful examination of the separate components of the time series.

In an attempt to capture the data's variability on timescales of years and greater, we ran the parameter optimization on two versions of the model that allowed interannual variability in the timing of leaf growth. We first performed an optimization in which the single D_{on} parameter was replaced by 10 parameters, one for each year. This modification led to a significant improvement in the optimized model-data fit. The best point found in this optimization had an RMS error of 0.937 g C m^{-2}, and a log likelihood that was 132.6 points better than the optimization on the unmodified model (Table 6). With nine additional parameters, however, the modified model is expected to perform better after optimization simply because it has more degrees of freedom. The Bayesian Information Criterion (BIC) can be used to select between two models with different numbers of parameters (Kendall & Ord, 1990):

$$\mathrm{BIC} = -2\mathrm{LL} + K \ln(n), \qquad (6)$$

where LL is the log likelihood, K is the number of parameters, and n is the number of data points. The model with the lower BIC is considered to be the better model. The BIC of the unmodified model was 10 471 and that of the modified model was 10 279. Thus, even after accounting for the difference in the number of parameters in this way, we still find that the modified model represents a significant improvement over the unmodified model. The retrieved values for D_{on} for each year from 1992 to 2001 showed a spread of about three weeks, from 132 (May 11) to 153 (June 2), suggesting the importance of accurately specifying phenological variability in models like SIPNET.

Next, we performed an optimization in which the date-based leaf growth was replaced by temperature-based growth. As in PnET, we parameterized leaf onset in terms of growing-degree day accumulation (GDD) since January 1 (Aber *et al.*, 1996). The number of parameters was the same in this version of the model, but the D_{on} parameter was replaced by a G_{on} parameter, which specified the GDD threshold at which leaves appeared. The initial guess for G_{on} was set at 500 °C-day with an allowable range from 100 to 900 °C-day, based on values given by Aber *et al.* (1996). The optimized version of this model performed significantly worse than the optimized unmodified model (Table 6). This result calls into question the modeling of phenological variability based on a GDD accumulation.

Interestingly, both modifications led to a slight *decrease* in the optimized model fit to the data's interannual variability (Table 6), the measure they were designed to improve upon. Capturing the data's interannual variability and trends will therefore most likely require the addition of model processes that operate on these time scales.

Conclusions

Net ecosystem carbon flux observations can be used to estimate parameters and initial conditions of an

13652486, 2005, 2, Downloaded from https://onlinelibrary.wiley.com/doi/10.1111/j.1365-2486.2005.00897.x by University Of Arizona Library, Wiley Online Library on [24/07/2024]. See the Terms and Conditions (https://onlinelibrary.wiley.com/terms-and-conditions) on Wiley Online Library for rules of use; OA articles are governed by the applicable Creative Commons License

appropriately formulated model, providing insight into both the data and the model. Our approach has the advantage that the retrieved parameter values are mutually consistent with each other because they are estimated simultaneously. In contrast, estimation approaches that estimate the parameters independently ignore parameter covariances, and so may yield suboptimal solutions. The parameters also share a common error budget, allowing for simple propagation and attribution of uncertainty. It is relatively straightforward to determine the uncertainty both of the individual parameters and of the posterior estimates of NEE. The issue of uniqueness of the solution is also explicitly addressed because parameters that are highly correlated with one another can be identified in the analysis.

Curve-fitting analyses often find that different respiration temperature coefficients are needed for different times of the year or for diurnal vs. seasonal responses because of changes in biogeochemical state variables (Yuste *et al*., 2004). Our approach, by capturing the first-order nature of ecosystem processes through compartment modeling, estimates a single set of physiological parameters that fit well on diurnal and seasonal timescales (Fig. 8). Our modeling approach thus successfully captured those timescales where carbon exchange is strongly forced by the energy budget. Timescales where the more stochastic precipitation-related processes and internal ecosystem dynamics dominate were captured much less successfully. These timescales (weeks to months and seasons to years) have lower signals relative to noise, and are governed by more complex ecosystem processes, including time-lagged responses to environmental changes (Schimel *et al*., 2005). Capturing the processes governing these time scales will require, at least, longer time-series, a more sophisticated model, improved fitting procedures to capture the smaller signals of the synoptic and interannual timescales, and the use of additional data types (e.g. water vapor fluxes, soil chamber data and carbon stock measurements) in a multivariate approach.

The assimilation approach also addresses scaling issues. Ideally, parameters and initial conditions for ecosystem models are directly measured in experimental studies. However, even in the best cases, these estimates are uncertain, and in the worst cases, no direct measurement technique exists. In virtually all cases, parameters must be scaled up from laboratory or field experiments to much larger areas. Given the typical high degree of uncertainty in measuring and scaling direct parameter estimates, assimilation can help locate parameter values that lie within the biophysically possible ranges that maximize the overall fit to flux data. This process aids in both minimizing the impact of experimental uncertainty in estimating parameters, and in scaling them to the appropriate level. In the case of parameters, where no direct measurement technique exists (e.g. processes that operate too slowly for typical field studies), values may be estimated that are consistent with the flux observations. In this way, assimilation is an important complement to experimental studies and can be used to statistically link experiments and flux data sets.

Finally, it is important to emphasize that parameter estimation techniques, such as the approach used in this paper, which allow synthesis of data with complex models that potentially have a large number of parameters, can lead to overfitting. In addition to the usual statistical cautions associated with fitting problems, we recommend beginning with the simplest possible models based on well-understood processes, and adding additional mechanisms only when justified by theory and/or process measurements. An initial fit to a complex model with a small residual error leaves little room for additional hypothesis testing.

Acknowledgments

The CO_2 eddy flux and meteorological data used in this study were collected, maintained, and generously provided by Steve Wofsy and colleagues affiliated with the Harvard Forest Environmental Measurement Site. We are grateful to Shawn Urbanski for his helpful comments on this manuscript. We also thank Scott Ollinger for helpful discussions about PnET model parameters. We gratefully acknowledge George Hurtt and the joint NASA-UNH Research and Discover Program for bringing Bill Sacks into this project. Thanks to Steve Aulenbach for suggesting the wavelet analysis. This paper represents the initial results of our NASA grant (NAG5-12876) to study ecosystem flux data assimilation, and was supported in part by a NASA Interdisciplinary Science team grant to UNH. The National Center for Atmospheric Research is funded by the National Science Foundation.

References

Aber JD, Federer CA (1992) A generalized, lumped-parameter model of photosynthesis, evapo-transpiration and net primary production in temperate and boreal forest ecosystems. *Oecologia*, **92**, 463–474.

Aber JD, Magill A, Boone R *et al*. (1993) Plant and soil responses to chronic nitrogen additions at the Harvard Forest, Massachusetts. *Ecological Applications*, **3**, 156–166.

Aber JD, Ollinger SV, Driscoll CT (1997) Modeling nitrogen saturation in forest ecosystems in response to land use and atmospheric deposition. *Ecological Modelling*, **101**, 61–78.

Aber JD, Ollinger SV, Federer CA *et al*. (1995) Predicting the effects of climate change on water yield and forest production in the northeastern United States. *Climate Research*, **5**, 207–222.

Aber JD, Reich PB, Goulden ML (1996) Extrapolating leaf CO_2 exchange to the canopy: a generalized model of forest

13652486, 2005, 2, Downloaded from https://onlinelibrary.wiley.com/doi/10.1111/j.1365-2486.2005.00897.x by University Of Arizona Library, Wiley Online Library on [24/07/2024]. See the Terms and Conditions (https://onlinelibrary.wiley.com/terms-and-conditions) on Wiley Online Library for rules of use; OA articles are governed by the applicable Creative Commons License

photosynthesis validated by eddy correlation. *Oecologia*, **106**, 257–265.

Baldocchi DD, Hicks BB, Meyers TP (1988) Measuring biosphere–atmosphere exchanges of biologically related gases with micrometeorological methods. *Ecology*, **69**, 1331–1340.

Baldocchi DD, Wilson KB (2001) Modeling CO_2 and water vapor exchange of a temperate broadleaved forest across hourly to decadal time scales. *Ecological Modelling*, **142**, 155–184.

Barford CC, Pyle EH, Hutyra L *et al*. (2001a) *Leaf Area Index measurements*. ftp://ftp.as.harvard.edu/pub/nigec/HU_Wofsy/hf_data/ecological_data/lai.hf.txt (accessed July 2002).

Barford CC, Wofsy SC, Goulden ML *et al*. (2001b) Factors controlling long- and short-term sequestration of atmospheric CO_2 in a mid-latitude forest. *Science*, **294**, 1688–1691.

Bishop C (1995) *Neural Networks for Pattern Recognition*. Oxford University Press, New York.

Curtis PS, Hanson PJ, Bolstad P *et al*. (2002) Biometric and eddy-covariance based estimates of annual carbon storage in five eastern North American deciduous forests. *Agricultural and Forest Meteorology*, **113**, 3–19.

Edwards NT, Hanson PJ (1996) Stem respiration in a closed-canopy upland oak forest. *Tree Physiology*, **16**, 433–439.

Falge E, Baldocchi DD, Olson RJ *et al*. (2001) Gap filling strategies for long term energy flux data sets. *Agricultural and Forest Meteorology*, **107**, 71–77.

Gelman AB, Carlin JS, Stern HS *et al*. (1995) *Bayesian Data Analysis*. Chapman & Hall, Florida.

Giardina CP, Ryan MG (2000) Evidence that decomposition rates of organic carbon in mineral soil do not vary with temperature. *Nature*, **404**, 858–861.

Goulden ML, Munger JW, Fan SM *et al*. (1996) Measurements of carbon sequestration by long-term eddy covariance: methods and a critical evaluation of accuracy. *Global Change Biology*, **2**, 169–182.

Graps A (1995) An introduction to wavelets. *IEEE Computational Sciences and Engineering*, **2**, 50–61.

Hastings WK (1970) Monte Carlo sampling methods using Markov chains and their applications. *Biometrika*, **57**, 97–109.

Hurtt GC, Armstrong RA (1996) A pelagic ecosystem model calibrated with BATS data. *Deep-Sea Research Part II-Topical Studies in Oceanography*, **43**, 653–683.

Kendall MG, Ord JK (1990) *Time Series*. Oxford University Press, New York.

Lau KM, Weng HY (1995) Climate signal detection using wavelet transform: how to make a time series sing. *Bulletin of the American Meteorological Society*, **76**, 2391–2402.

Law BE, Sun OJ, Campbell J *et al*. (2003) Changes in carbon storage and fluxes in a chronosequence of ponderosa pine. *Global Change Biology*, **9**, 510–524.

Luo YQ, Wu LH, Andrews JA *et al*. (2001) Elevated CO_2 differentiates ecosystem carbon processes: deconvolution analysis of Duke Forest FACE data. *Ecological Monographs*, **71**, 357–376.

MacKay DJC (1992) A practical Bayesian framework for back-propagation networks. *Neural Computation*, **4**, 448–472.

Magill AH, Aber JD, Berntson GM *et al*. (2000) Long-term nitrogen additions and nitrogen saturation in two temperate forests. *Ecosystems*, **3**, 238–253.

Metropolis N, Rosenbluth AW, Rosenbluth MN *et al*. (1953) Equations of state calculations by fast computing machines. *Journal of Chemical Physics*, **21**, 1087–1092.

Parton WJ, Hartman M, Ojima D *et al*. (1998) DAYCENT and its land surface submodel: description and testing. *Global and Planetary Change*, **19**, 35–48.

Potter CS, Randerson JT, Field CB *et al*. (1993) Terrestrial ecosystem production: a process model based on global satellite and surface data. *Global Biogeochemical Cycles*, **7**, 811–841.

Radtke PJ, Burk TE, Bolstad PV (2001) Estimates of the distributions of forest ecosystem model inputs for deciduous forests of eastern North America. *Tree Physiology*, **21**, 505–512.

Raich JW, Rastetter EB, Melillo JM *et al*. (1991) Potential net primary productivity in South-America: application of a global model. *Ecological Applications*, **1**, 399–429.

Reichstein M, Rey A, Freibauer A *et al*. (2003) Modeling temporal and large-scale spatial variability of soil respiration from soil water availability, temperature and vegetation productivity indices. *Global Biogeochemical Cycles*, **17**, 1104, doi: 10.1029.

Ryan MG, Law BE (in press) Interpreting, measuring and modeling soil respiration. *Biogeochemistry*.

Schimel DS, Churkina G, Braswell BH, Trembath J (in press) Remembrance of weather past: ecosystem response to climate variability. In: *A History of Atmospheric CO_2 and its Effects on Plants, Animals and Ecosystems* (eds. Ehleringer J, Cerling TE, Dearing MD), Springer-Verlag, Berlin.

Torrence C, Compo GP (1998) A practical guide to wavelet analysis. *Bulletin of the American Meteorological Society*, **79**, 61–78.

Vukicevic T, Braswell BH, Schimel DS (2001) A diagnostic study of temperature controls on global terrestrial carbon exchange. *Tellus (B)*, **53**, 150–170.

Wofsy SC, Goulden ML, Munger JW *et al*. (1993) Net exchange of CO_2 in a mid-latitude forest. *Science*, **260**, 1314–1317.

Yuste JC, Janssens IA, Carerra A *et al*. (2004) Annual Q10 of soil respiration reflects plant phenological patterns as well as temperature sensitivity. *Global Change Biology*, **10**, 161–170.

Appendix A: Model Description

SIPNET contains two vegetation carbon pools (leaves and wood) and an aggregated soil carbon pool, as well as a simple soil moisture sub-model (Fig. 1). The carbon stored in leaves is assumed to remain constant throughout the growing season, and thus photosynthesis and autotrophic respiration affect only the amount of carbon stored in the plant wood carbon pool. Although this is a somewhat unrealistic assumption, we applied this simplification – and other simplifications – to reduce the number of free parameters in the optimization and to ease the diagnosis of model-data errors. Furthermore, using a too complex model in the optimization could lead to over-fitting, which would reduce the number of informative model-data errors, and thus reduce the amount that could be learned from the optimization exercise. This point is especially

13652486, 2005, 2, Downloaded from https://onlinelibrary.wiley.com/doi/10.1111/j.1365-2486.2005.00897.x by University Of Arizona Library, Wiley Online Library on [24/07/2024]. See the Terms and Conditions (https://onlinelibrary.wiley.com/terms-and-conditions) on Wiley Online Library for rules of use; OA articles are governed by the applicable Creative Commons License

relevant regarding processes such as leaf carbon allocation for which the governing equations themselves are highly uncertain.

The model evolves according to the following equations:

$$\frac{dC_W}{dt} = GPP - R_a - L_W - L, \quad (A1)$$

$$\frac{dC_L}{dt} = L - L_L, \quad (A2)$$

$$\frac{dC_S}{dt} = L_W + L_L - R_h, \quad (A3)$$

$$\frac{dW}{dt} = P - T - D, \quad (A4)$$

where C_W is the plant wood carbon ($g\,C\,m^{-2}$), C_L is plant leaf carbon ($g\,C\,m^{-2}$), C_S is soil carbon ($g\,C\,m^{-2}$), W is soil water storage (cm), t is time (day), GPP is gross photosynthesis, R_a is autotrophic respiration, L_W is wood litter, L is leaf creation, L_L is leaf litter, R_h is heterotrophic respiration, P is precipitation, T is transpiration, and D is drainage. All carbon fluxes have units of $g\,C\,m^{-2}\,day^{-1}$, and all water fluxes have units of cm water equivalence day^{-1}. These fluxes are described in detail in the sections below.

Photosynthesis

As in PnET (Aber & Federer, 1992), photosynthesis is calculated as a maximum gross photosynthetic rate multiplied by four scalars, each between 0 and 1: a temperature factor (D_{temp}), a VPD factor (D_{VPD}), a light factor (D_{light}), and a water factor (D_{water}). To calculate the maximum photosynthetic rate, A_{max} (the leaf-level maximum net instantaneous CO_2 assimilation rate) is first divided into gross photosynthesis and foliar respiration. As in Aber & Federer (1992), foliar respiration is assumed to be proportional to A_{max}:

$$R_{f,o} = K_F A_{max}, \quad (A5)$$

where $R_{f,o}$ is the foliar maintenance respiration rate at T_{opt} ($nmol\,CO_2\,g^{-1}$ leaf s^{-1}).

A_{max} represents the maximum photosynthetic rate in the early morning, when this rate is at its peak. The maximum rate over a whole day is somewhat lower, and this is taken into account by multiplying A_{max} by a scaling factor, A_d (Aber *et al*., 1996). Thus, SIPNET calculates the daily maximum *gross* photosynthetic rate, GPP_{max} ($nmol\,CO_2\,g^{-1}$ leaf s^{-1}), as in Aber *et al*. (1996):

$$GPP_{max} = A_{max} A_d + R_{f,o}. \quad (A6)$$

The reductions of GPP_{max} due to air temperature (T_{air}), VPD, light and water are performed in two stages. First a potential photosynthetic rate is calculated assuming no water stress (GPP_{pot}). Then this water stress-free value is used in the calculation of water stress, and the water stress is applied. Again, the scheme used is the same as that used in PnET (Aber & Federer, 1992):

$$GPP_{pot} = GPP_{max} D_{temp} D_{VPD} D_{light}, \quad (A7)$$

GPP_{pot} is then converted into units of $g\,C\,m^{-2}$ (ground) day^{-1} using SLW and LAI, where LAI is the current LAI (m^2 (leaf) m^{-2} (ground)), given by

$$LAI = \frac{C_L}{SLW\,C_{frac}}, \quad (A8)$$

D_{temp}, which determines the effect of temperature on photosynthesis, is assumed to be a parabolic function, with a value of 1 when $T_{air} = T_{opt}$ and a value of 0 when $T_{air} \le T_{min}$ or $T_{air} \ge T_{max}$, as in Aber & Federer (1992):

$$D_{temp} = Max\left(\frac{(T_{max} - T_{air})(T_{air} - T_{min})}{((T_{max} - T_{min})/2)^2}, 0\right), \quad (A9)$$

D_{VPD} expresses the decrease in leaf gas exchange – both photosynthesis and transpiration – due to VPD (Aber & Federer, 1992; Aber *et al*., 1996). The following empirical relationship is used for D_{VPD}, from Aber *et al*. (1996):

$$D_{VPD} = 1 - K_{VPD}\,VPD^2. \quad (A10)$$

The D_{light} multiplier expresses the actual amount of light absorbed per unit leaf area as a fraction of the ideal maximum light absorption. The calculation of D_{light} takes into account both the amount of light falling on the top of the canopy in a given day (the amount of PAR) and the attenuation of light as it filters down through the canopy. The scheme presented in Aber & Federer (1992) is employed, numerically approximating the integral of the light absorption through the entire canopy by considering 50 distinct layers.

At each layer i, the cumulative LAI (LAI_i) is calculated as the LAI from level i up, assuming that the layers are homogeneous. The light intensity at a given layer, I_i (Einsteins $m^{-2}\,day^{-1}$), is given by the PAR decreased by the light attenuation down to that layer:

$$I_i = PAR\,e^{-k\,LAI_i}. \quad (A11)$$

The light effect for a given layer ($D_{light,i}$) is a number between 0 and 1, increasing with increasing I_i:

$$D_{light,i} = 1 - e^{-(I_i \ln(2)/PAR_{1/2})}. \quad (A12)$$

The cumulative light effect over the entire canopy is the mean of the light effects at each layer.

D_{water}, the decrease in photosynthesis due to soil dryness, is also calculated as in Aber & Federer (1992). The plants' WUE ($mg\,CO_2\,g^{-1}\,H_2O$), depends on VPD. The potential transpiration (T_{pot}) – that is, the level of transpiration possible with moisture-saturated soil – depends on GPP_{pot} (the level of photosynthesis without

13652486, 2005, 2, Downloaded from https://onlinelibrary.wiley.com/doi/10.1111/j.1365-2486.2005.00897.x by University Of Arizona Library, Wiley Online Library on [24/07/2024]. See the Terms and Conditions (https://onlinelibrary.wiley.com/terms-and-conditions) on Wiley Online Library for rules of use; OA articles are governed by the applicable Creative Commons License

water stress) and WUE:

$$\mathrm{WUE} = \frac{K_{\mathrm{WUE}}}{\mathrm{VPD}}, \tag{A13}$$

$$T_{\mathrm{pot}} = \frac{\mathrm{GPP}_{\mathrm{pot}}}{\mathrm{WUE}}, \tag{A14}$$

T_{pot} is then converted into units of cm $H_2O\,\mathrm{day}^{-1}$. The total amount of water available to the plants over the course of a day (W_a) is a fraction (f) of the total amount of water in the soil (W). Actual transpiration (T) is then given by

$$T = \mathrm{Min}(T_{\mathrm{pot}},\ W_{\mathrm{a}}). \tag{A15}$$

Finally, D_{water} is calculated as

$$D_{\mathrm{water}} = \frac{T}{T_{\mathrm{pot}}}. \tag{A16}$$

The total adjusted GPP is then

$$\mathrm{GPP} = \mathrm{GPP}_{\mathrm{pot}}\, D_{\mathrm{water}}. \tag{A17}$$

Note that it will often be the case that $T = T_{\mathrm{pot}}$, making $D_{\mathrm{water}} = 1$ and $\mathrm{GPP} = \mathrm{GPP}_{\mathrm{pot}}$.

Autotrophic and heterotrophic respiration

Autotrophic respiration in SIPNET (R_a) is the sum of two terms: foliar maintenance respiration, R_f, and wood maintenance respiration, R_m. Growth respiration is not explicitly modeled, but rather is implicitly included in the maintenance respiration term.

$R_{f,o}$ represents the foliar respiration rate at the optimum temperature for photosynthesis, as described above. Actual foliar respiration is determined using a Q_{10} function:

$$R_{\mathrm{f}} = R_{\mathrm{f,o}} {Q_{10\mathrm{v}}}^{(T_{\mathrm{air}} - T_{\mathrm{opt}})/10}. \tag{A18}$$

R_f is then converted into units of $\mathrm{g\,C\,m^{-2}}$ (ground) day^{-1}.

Wood maintenance respiration ($\mathrm{g\,C\,m^{-2}\,day^{-1}}$) is calculated as a function of wood carbon content and T_{air}, as in TEM (Raich *et al.*, 1991). The same Q_{10} value is used as that used for foliar respiration, but the base wood respiration is expressed as the rate at 0 °C, giving:

$$R_{\mathrm{m}} = K_{\mathrm{A}} C_{\mathrm{W}} {Q_{10\mathrm{v}}}^{T_{\mathrm{air}}/10}. \tag{A19}$$

Heterotrophic respiration (R_h) is calculated as in PnET-CN (Aber *et al.*, 1997), as a function of soil carbon content, soil temperature (T_{soil}) and soil moisture:

$$R_{\mathrm{h}} = C_{\mathrm{S}}\, K_{\mathrm{H}} {Q_{10\mathrm{s}}}^{T_{\mathrm{soil}}/10}\, (W/W_c). \tag{A20}$$

Phenology and Litterfall

Rather than using a complex phenology and carbon allocation scheme, a simple time-based function is used for leaf growth. On a specified day of the year (D_{on}), all the leaves appear in a single time step. LAI is constant from year-to-year, and is specified by L_{max}. The amount of carbon transferred from wood to leaves is calculated based on L_{max}, SLW and C_{frac}.

Litterfall is the sum of two terms in SIPNET: wood litter and leaf litter. Like leaf creation, leaf litter is governed by a simple time-based function. On a specified day of the year (D_{off}), all the leaves fall off in a single time step. Wood litter is assumed to be a constant fraction of total wood carbon, with the rate of transfer determined by K_{W}.

Soil Moisture

Soil moisture affects both the heterotrophic respiration rate and the realized gross photosynthetic rate in SIPNET. A simple bucket model is employed to track the change in soil-held water over time, based on the soil moisture model in PnET (Aber & Federer, 1992). The single water flux into the system is precipitation and the two fluxes out are transpiration and drainage. Initial tests demonstrated that the separation of precipitation into rain and snow had little effect on the model, so all precipitation is assumed to fall as rain. Transpiration is dependent on the amount of water available to vegetation and on the potential (i.e. water stress-free) level of photosynthesis, as described above. The drainage term is equivalent to an overflow of the bucket: if the amount of water in the soil would exceed the water holding capacity (W_c), all water in excess of W_c is removed by drainage.

Appendix B: Method used for estimation of process model parameters

The procedure we have used is an iterative Bayesian calculation, assuming independent Gaussian error distributions. In this discussion we use the concept of likelihood L, defined as

$$L(y|\boldsymbol{\theta}) = (\mathrm{data}|\mathrm{model}) \sim \mathrm{Normal} \tag{B1}$$

where the model estimate of the data, in this case net ecosystem exchange, depends upon a set of parameters $\boldsymbol{\theta}$. We assume that the joint posterior probability distribution function of the parameter vector $\boldsymbol{\theta} = (\boldsymbol{\theta}_1, \ldots, \boldsymbol{\theta}_k)$ is analytically intractable. Therefore the goal is to generate a Monte Carlo sample from the joint posterior distribution. In Bayesian estimation typically only a scalar multiple of the posterior distribution is available in analytical form as a result of Bayes' theorem,

$$f(\boldsymbol{\theta}|y) = L(y|\boldsymbol{\theta})\, p(\boldsymbol{\theta})/c, \tag{B2}$$

where $p(\boldsymbol{\theta})$ is the prior distribution, $\mathrm{L}(y|\boldsymbol{\theta})$ is the likelihood (joint pdf of the data y given parameter value $\boldsymbol{\theta}$), and the scalar multiple c is the

13652486, 2005, 2, Downloaded from https://onlinelibrary.wiley.com/doi/10.1111/j.1365-2486.2005.00897.x by University Of Arizona Library, Wiley Online Library on [24/07/2024]. See the Terms and Conditions (https://onlinelibrary.wiley.com/terms-and-conditions) on Wiley Online Library for rules of use; OA articles are governed by the applicable Creative Commons License

normalizing constant,

$$c = \int \int L(y|\boldsymbol{\theta}) p(\boldsymbol{\theta})\, d\boldsymbol{\theta}. \tag{B3}$$

This multiple integration is numerically taxing for moderate to large numbers of parameters k, and exhaustive grid sampling for large k requires many calculations of the likelihood (which are based upon process model runs in our case).

We utilize samples from a MC as substitutes for random samples. The MCMC approach is an efficient way of sampling $\boldsymbol{\theta}$ from its posterior distribution by only visiting relevant regions of that distribution. MCMC requires evaluation of the numerator $\mathrm{L}(y|\boldsymbol{\theta})\,\mathrm{p}(\boldsymbol{\theta})$ in Bayes' theorem, but not the denominator. Thus no expensive Monte Carlo integration of c in Eqn (2) is necessary. MCMC uses ergodic MC samples to explore the parameter space. These are not random samples. However, they are identically distributed after a burn-in period, and therefore their sample moments (expected values) converge to corresponding population (distribution) moments when large sample sizes are used. Hence the means, standard deviations, and quantiles of the MC samples can be taken reliably (after the burn-in period) for estimation purposes.

The Metropolis Algorithm

Ergodic MCs are MCs where each state can be visited from any other states with positive probability. An ergodic MC has a stationary distribution: After many steps, the probability of reaching any state in the next step remains approximately constant. These probabilities are called the equilibrium, or stationary distribution of the MC.

For discrete MCs with transition matrix $\mathbf{M}$ with elements $M_{ij} = \mathrm{Prob}(X_j|X_i)$ the stationary distribution $\mathbf{p} = (p_1, \ldots)$ (row vector) is defined by $\mathbf{p} = \mathbf{pM}$. For continuous MCs, with a transition distribution $J(v|u)$ that moves u to a value v, the stationary distribution function $f_{\mathrm{stat}}(\cdot)$ is defined by

$$f_{\mathrm{stat}}(v) = \int J(v|u) f_{\mathrm{stat}}(u)\mathrm{d}u;\ (\text{for all } u \text{ and } v). \tag{B4}$$

We can show that the reversibility condition implies that f_{stat} is a stationary distribution:

$$\begin{aligned}\int J(v|u) f_{\mathrm{stat}}(u)\mathrm{d}u &= \int J(u|v) f_{\mathrm{stat}}(v)\mathrm{d}u \\ &= f_{\mathrm{stat}}(v) \int J(u|v)\mathrm{d}u = f_{\mathrm{stat}}(v).\end{aligned} \tag{B5}$$

Therefore, when we construct a chain for MCMC, we simply need to show that the reversibility holds, from which, in turn, the stationarity holds. The Metropolis Algorithm (using notation related to process model parameter estimation) consists of the following:

Step 1: Construct a symmetric, proposal transition pdf from $\boldsymbol{\theta}_i$ to $\boldsymbol{\theta}_k$, such that $\mathrm{M}(\boldsymbol{\theta}_k|\boldsymbol{\theta}_i) = \mathrm{M}(\boldsymbol{\theta}_i|\boldsymbol{\theta}_k)$.

Step 2: Accept $\boldsymbol{\theta}_k$ with probability $a = \min[1, \mathrm{f}(\boldsymbol{\theta}_k|y)/\mathrm{f}(\boldsymbol{\theta}_i|y)]$. Note that Step 2 can be executed by drawing U from a Uniform $(0, 1)$ and accepting $\boldsymbol{\theta}_k$ if $U \le \mathrm{f}(\boldsymbol{\theta}_k|y)/\mathrm{f}(\boldsymbol{\theta}_i|y) = \mathrm{L}(y|\boldsymbol{\theta}_k)\,\mathrm{p}(\boldsymbol{\theta}_k)/\mathrm{L}(y|\boldsymbol{\theta}_i)\,\mathrm{p}(\boldsymbol{\theta}_i)$.

Why the Metropolis algorithm works

We need to prove the reversibility condition for the Metropolis algorithm:

Letting $u = \boldsymbol{\theta}_i$ and $v = \boldsymbol{\theta}_k$ and $f(u) = f(\boldsymbol{\theta}_i|y)$, we can see that the Metropolis algorithm produces an ergodic chain with transition pdf proportional to $a\ M(v|u)$ where a is the acceptance probability. But now we see that

$$\begin{aligned}J(v|u)f(u) &= \min[1, f(v)/f(u)]\mathrm{M}(v|u)\, f(u) \\ &= \min[f(u), f(v)]\, \mathrm{M}(v|u) \\ &= \min[f(u), f(v)]\mathrm{M}(u|v) \\ &= f(v)\min[1, f(u)/f(v)]\mathrm{M}(u|v) \\ &= \mathrm{J}(u|v)\, f(v).\end{aligned} \tag{B6}$$

Several practical issues must be considered when applying this MCMC algorithm. The most common symmetric proposal distributions are the multivariate normal or multivariate t distributions with mean equal to the current state. For the multivariate normal proposal distribution, the best scale (variance covariance matrix of the jumping distribution) is a scalar fraction of the posterior variance–covariance matrix. Of course finding the correct scale requires tuning. An overall acceptance rate of about 40% has been found to be reasonable in many applications.

Hastings (1970) proposed a generalization to the Metropolis algorithm, the so-called Metropolis–Hastings algorithm that uses a general nonsymmetric transition probability $J(y|x)$. The algorithm requires a slightly more complicated acceptance ratio in the form of:

Accept a proposal $\boldsymbol{\theta}_k$ if $U \le J(\boldsymbol{\theta}_k|\boldsymbol{\theta}_i)\, L(y|\boldsymbol{\theta}_k)\, p(\boldsymbol{\theta}_k)/J(\boldsymbol{\theta}_i/\boldsymbol{\theta}_k)\, L(y|\boldsymbol{\theta}_i)\, p(\boldsymbol{\theta}_i)$.

13652486, 2005, 2, Downloaded from https://onlinelibrary.wiley.com/doi/10.1111/j.1365-2486.2005.00897.x by University Of Arizona Library, Wiley Online Library on [24/07/2024]. See the Terms and Conditions (https://onlinelibrary.wiley.com/terms-and-conditions) on Wiley Online Library for rules of use; OA articles are governed by the applicable Creative Commons License